

1

**AD-A273 743**



**S DTIC**  
**ELECTE**  
**DEC 16 1993**  
**A**

**A THEORETICAL INVESTIGATION OF  
ELECTRICALLY TUNABLE BIREFRINGENT  
OPTICAL FILTERS AS THE SPECTRAL  
DISCRIMINATOR IN HYPERSPECTRAL  
IMAGING SYSTEMS**

**THESIS**

**Duane A. Sauve, Captain, USAF**

**AFIT/GEO/ENP/93D-02**

**93-30495**



Approved for public release; distribution unlimited

**93 12 1 5 1 1 3**

**A THEORETICAL INVESTIGATION OF ELECTRICALLY TUNABLE  
BIREFRINGENT OPTICAL FILTERS AS THE SPECTRAL DISCRIMINATOR IN  
HYPERSPECTRAL IMAGING SYSTEMS**

**THESIS**

**Presented to the Faculty of the Graduate School of  
Engineering of the Air Force Institute of Technology**

**Air University**

**In Partial Fulfillment of the Requirements for the Degree of  
Master of Science in Electrical Engineering**

**Duane A. Sauve, B. S.**

**Captain, USAF**

**December 1993**

**Approved for public release; distribution unlimited**

## Preface

The purpose of study was to investigate electrically tunable birefringent optical filters for use as the spectral discriminator in hyperspectral imaging systems. Richard Fedors of Rome Laboratory in New York originated this thesis topic as a possible way to decrease the complexity of spectral discrimination for multispectral imaging systems.

Analytical and computer analysis was performed for known birefringent filters which show promise of electrical tunability, excluding acousto-optic filters. No perfect match was found to the ideal tunable optical filter for hyperspectral imaging defined in this thesis; however, this thesis provides the needed background for further research in this area. This thesis also identifies a number of areas for further worthwhile research.

This thesis effort was not an individual one. First, I acknowledge and thank my creator. I also thank my faculty advisor Dr. T. E. Luke for helping me to refocus when progress slowed. Words of thanks are also owed to the AFIT library staff for their professionalism and responsiveness to my many requests. Finally, I thank my wife Stephanie for all of the encouragement and support during the AFIT experience.

Duane A. Sauve

Accession For	
NTIS	CRA&I
DTIC	TAB
Unannounced	
Justification	
By	
Distribution /	
Availability Codes	
Dist	Avail and/or Special
A-1	

## Table of Contents

	Page
Preface	ii
List of Figures	v
List of Tables	viii
Abstract	ix
I. Introduction	1
Problem Statement	1
Electrically Tunable Birefringent Optical Filters	1
HI Systems	2
Multispectral Image Formation	2
Spatial Information	3
Spectral Information	3
Scanning Versus Staring	6
Scanning Systems	6
Staring Systems	7
A Comparison	7
The Representative HI System and the Ideal Filter	8
The Representative HI Systems	8
The Ideal TOF for Spectral Discrimination in HI Applications	9
Methodology	9
Assumptions and Limitations	10
II. Lyot Based Filters	12
Introduction	12
The Lyot Birefringent Filter	12
The Single Stage Lyot Filter	12
The Multiple Stage Lyot Filter	16
Transmission profile of the Lyot Filter	18
The $\Delta n$ -tuned Lyot Filter	19
Tuning Mechanism	19
Tuning Characteristics	19
Operation in the HI spectral region	19
The Wave-Plate-Tuned Lyot Filter	23
Tuning Mechanism	23
Tuning Characteristics	24
Operation in the HI spectral region	25

Pass Band Shaping with Lyot Type Filters	27
The Contrast Element	27
Non-standard Plate Thickness	27
Arbitrary Pass Band Shapes	28
<b>III. Solc Based Filters</b>	<b>30</b>
Introduction	30
The Solc Birefringent Filter	30
The $\Delta n$ -tuned Solc Filter	34
Tuning Mechanism	34
Tuning Characteristics	34
Operation in the HI spectral region	35
The Wave-Plate-Tuned Solc Filter	35
Tuning Mechanism	35
Tuning Characteristics	37
Operation in the HI spectral region	37
The Electro-optic Tunable Filter (EOTF)	39
Tuning Mechanism	39
Tuning Characteristics	42
Operation in the HI spectral region	43
Pass Band Shaping with Solc-type Filters	45
Solc Sections Joined with Polarizers	45
Optical Network Synthesis	46
<b>IV. Conclusions and Recommendations</b>	<b>48</b>
Introduction	48
Conclusions for Tunable Optical Filters	48
The $\Delta n$ -tuned Lyot Filter	48
The Wave-plate-tuned Lyot Filter	48
The $\Delta n$ -tuned Solc Filter	49
The Wave-plate-tuned Solc Filter	49
The EOTF	49
Pass Band Shaping Filters	50
Recommendations for Further Research	51
General Considerations	51
Filter Research	51
Material Research	51
Other Research	52
<b>Bibliography</b>	<b>53</b>
<b>Vita</b>	<b>57</b>

## List of Figures

Figure	Page
1. A Multispectral Image	3
2. Three Ways to Gather Spatial Information From an Object	4
3. Pushbroom Scanning to Form a Multispectral Image	4
4. Staring System with Sequential Spectral Information	5
5. Filter Wheel with Eight Spectral Bands	5
6. A Single Lyot Filter Element	13
7. Plot Showing Elliptical Polarization	14
8. Polarization Plots with $E_{ox} = E_{oy}$ for Various Values of $\epsilon$	14
9. Transmission Spectrum for a One Stage, Parallel Polarizer, Lyot Filter	15
10. A Two Stage Lyot Filter	16
11. Transmission vs. Frequency for (a) The First Stage of a Lyot (b) The Second Stage of a Lyot (c) The Two Stages Cascaded Together (Two Stage Lyot Filter)	17
12. Tuning Characteristics for a 5-stage $\Delta n$ -tuned Lyot Filter in the Visible Region	21
13. One Stage Lyot Filter Tuned with Achromatic Wave Plates	23
14. Linear Polarization Angle Change Through a Half-wave Plate	24
15. Tuning Characteristics for a 5-stage Wave-plate-tuned Lyot Filter in the Visible to Near-infrared Region	26
16. Side Lobe Suppression Using a Contrast Element (a) 5-stage Lyot Filter with No Contrast Element (b) 5-stage Lyot Plus a Contrast Element (6 stages total)	27

Figure	Page
17. Spectral Profile for (a) 5-stage Lyot Filter Non-standard Plate Thicknesses (b) Standard 5-stage Lyot	28
18. A Two Stage Lyot Filter with Lossy Polarizer	29
19. (a) A 4-stage Folded Solc Filter (b) A 4-stage Fan Solc Filter	31
20. Rotation of the Incoming x-polarized Light After Each Half-wave Plate in a 4-stage Solc Filter	33
21. Transmission Spectrum for 10-plate Fan and Folded Solc Filters with Randomly Polarized Input ( $\Delta n d = 600 \text{ nm}$ )	33
22. Tuning Characteristics for a 64-plate $\Delta n$ -tuned Solc Filter in the Visible to Near Infrared Region	36
23. Birefringent Plates for the Folded Solc Filter with Associated Tuning Sections for (a) The Positive Azimuth Angle Plates (b) The Negative Angle Plates	37
24. Tuning Characteristics for a 64-plate Wave-plate-tuned Solc Filter in the Visible to Near Infrared Region	38
25. A Transverse-field Electro-optic Tunable Filter Proposed in [22]	39
26. Voltage Waveform for Folded Solc Filter Operation, also Waveform for Shortest Pass Band Wavelength [22]	40
27. Sampled Sine Wave Azimuth Angle Distribution for a Solc Filter	41
28. Computer Simulation of Pass Band Splitting Close to $\lambda_f$ ( $\lambda_f = 400 \text{ nm}$ , $N =$ 48)	43
29. Tuning Characteristics for a 48-plate EOTF Filter with Randomly Polarized Input in the Visible to Near Infrared Region ( $\Delta n d = 190 \text{ nm}$ , $\rho_{\max}$ given by Equation 29)	43
30. Computer Simulation for Pass Band Center Wavelength versus Transmission at Pass Band Peak ( $\Delta n d = 190 \text{ nm}$ , $N = 48$ , $\rho_{\max}$ given by Equation 29)	44
31. Two 4-stage Solc filters Cascaded with a Polarizer	45

32. Computer Simulation contrasting Two 12-plate filters (a) Two 6-plate Solc Sections joined by a Polarizer (Plate thickness is  $d$  for one section and  $9d$  for the other) (b) One 12-plate Solc filter (thickness =  $d$  for all elements)



## List of Tables

Table	Page
1. Example of Channel Allocation for a $\Delta n$ -tuned Lyot Filter in the Visible Region	22
2. A Set of $\Delta n$ -tuned Lyot Filters Required to Tune Over the HI Spectrum	22
3. A Set of Wave-plate-tuned Lyot Filters Required to Tune Over the HI Spectrum	26
4. A Set of $\Delta n$ -tuned Solc Filters for the HI Spectrum	36
5. A Set of Wave-plate-tuned Solc Filters Required to Tune Over the HI Spectrum	38
6. A Set of EOTFs Required to Tune Over the HI Spectrum	44

### Abstract

This study investigated electrically tunable birefringent optical filters for use as the spectral discriminator in hyperspectral imaging systems. Spectral discrimination requirements for hyperspectral imaging systems were defined using specification from two state-of-the-art hyperspectral imaging systems. The spectral discrimination requirements led to the definition of the ideal tunable optical filter for spectral discrimination purposes. Analytical and computer analysis was performed for known birefringent filters which showed promise of electrical tunability, excluding acousto-optic filters. No perfect match was found to the ideal tunable optical filter for hyperspectral imaging defined in this thesis. Both Lyot and Solc based filters exhibited two drawbacks for hyperspectral imaging application: narrow tuning range with linear bandwidth dependence on center wavelength, or wide tuning range and quadratic bandwidth dependence on center wavelength. The  $\Delta$ -tuned Solc filter provided the best compromise between tuning range and bandwidth control; however, it is not practical due to the excessive number of elements required. This thesis provides the needed background for further research in this area and identifies a number of areas for further worthwhile research. Acousto-optic filters offer another possible avenue for hyperspectral imaging and should be investigated. Birefringent materials should also be studied to determine material limits on the electro-optic effect and spectral transmission characteristics to determine practical capabilities of filters discussed in this thesis.

# **A THEORETICAL INVESTIGATION OF ELECTRICALLY TUNABLE BIREFRINGENT OPTICAL FILTERS AS THE SPECTRAL DISCRIMINATOR IN HYPERSPECTRAL IMAGING SYSTEMS**

## **I. Introduction**

### **Problem Statement**

This thesis investigates electrically tunable birefringent optical filters for use as the spectral discriminator in hyperspectral imaging (HI) systems. This work defines the characteristics of a generic HI system based on current state-of-the-art HI systems and from these characteristics generates a hypothetical ideal tunable filter for HI. Existing filters, combinations of existing filters, and any filters originated during this thesis are characterized and compared to the ideal and to each other to determine their promise in HI applications. This thesis effort is not a detailed analysis of HI systems; however, some general properties of real world HI systems are used.

### **Electrically Tunable Birefringent Optical Filters**

An Electrically Tunable Birefringent Optical Filter (TOF) as discussed in this thesis is a device which selectively allows one optical spectral band to pass through it while blocking the rest of the optical spectrum. The TOF has a bandpass whose center frequency (or wavelength) is changed by alteration of the electrical signal applied to the filter. Most TOFs are based on the Lyot filter [1], the Solc filter [2], or the acousto-optic filter [3]. While the Lyot and Solc filters are not inherently tunable, the electro-optic effect or electrically rotatable waveplates can render them so. The acousto-optic filter is not considered in this thesis.

## HI Systems

HI systems are multispectral imaging systems with a large number of spectral channels (arbitrarily chosen to be greater than 100). Multispectral imaging is concerned with imaging remote objects (usually from an aircraft or spacecraft) both spatially and in several different spectral bands [4: 4]. An ordinary camera and several colored bandpass filters could form a multispectral image. One would simply take several snapshots of the same object, each snapshot with a different color filter attached to the camera. The multispectral image is the collection of all photographs of the same object; in this simplified example, a colored filter provides spectral discrimination. Most modern HI systems don't operate solely in the visible spectrum nor do they use photographic film to store image information; rather, they use some type of mass storage like optical disks or magnetic tape. Also, most existing HI systems use some combination of dichroic mirrors, gratings, prisms or a color wheel for spectral discrimination.

HI is important to both the military and civilian communities. The military is primarily concerned with remote target and threat detection and identification. Commercial interests are wide and varied; earth remote sensing systems look for wheat, minerals, schools of fish, pollution and more. The multispectral nature of the images helps to distinguish the object of interest from the background. For instance, a mobile missile launcher in a forested area might be invisible in the green spectral band but easily detectable in one of the infrared spectral bands. Similarly, a corn field imaged from a satellite might look the same as a prairie in one spectral band but different in another.

## Multispectral Image Formation

A multispectral image (Figure 1) has three dimensions: two of the dimensions are spatial and one dimension is spectral. The two spatial dimensions are the same as the spatial dimensions on an ordinary photograph. For a given multispectral image, there is

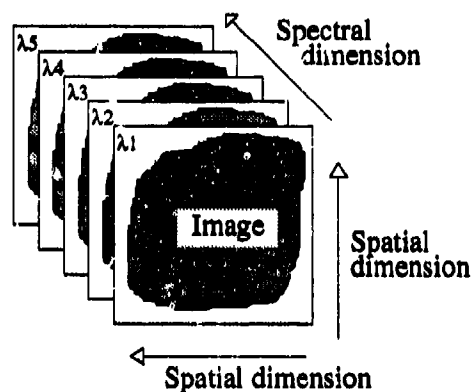


Figure 1. A Multispectral Image

one complete spatial image for every spectral channel. The multispectral image shown in Figure 1 has spatial information in five spectral bands.

*Spatial Information.* Let us set aside the spectral dimension for a moment and look at how a HI system gathers spatial image information (Figure 2). Each small square represents a single detector's instantaneous field of view (IFOV). In this example, a complete image frame consists of 64 IFOVs which make up one system field-of-view (SFOV). The scheme used in Figure 2a employs only one detector and mechanically scans the object in both spatial directions to construct a complete image. The method used in Figure 2b takes advantage of a 1 x 8 detector array to gather each row of IFOVs simultaneously while mechanically scanning the other spatial direction. A two-dimensional array can take both spatial dimensions simultaneously as shown in Figure 2c: no mechanical scanning is necessary; however, to image an area larger than the SFOV would require some type of scanning. Systems capable of gathering an entire SFOV with no mechanical scanning are called staring systems.

*Spectral Information.* Spectral information can be taken sequentially (one spectral band at a time) or in parallel (several spectral bands at the same time). The pushbroom method (Figure 3) is a state-of-the-art method for gathering spectral information in parallel. In the pushbroom scheme, one row of spatial IFOVs from the object is imaged

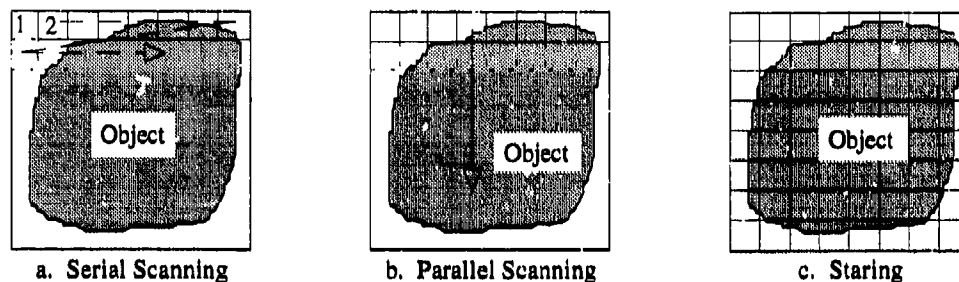


Figure 2. Three Ways to Gather Spatial Information From an Object

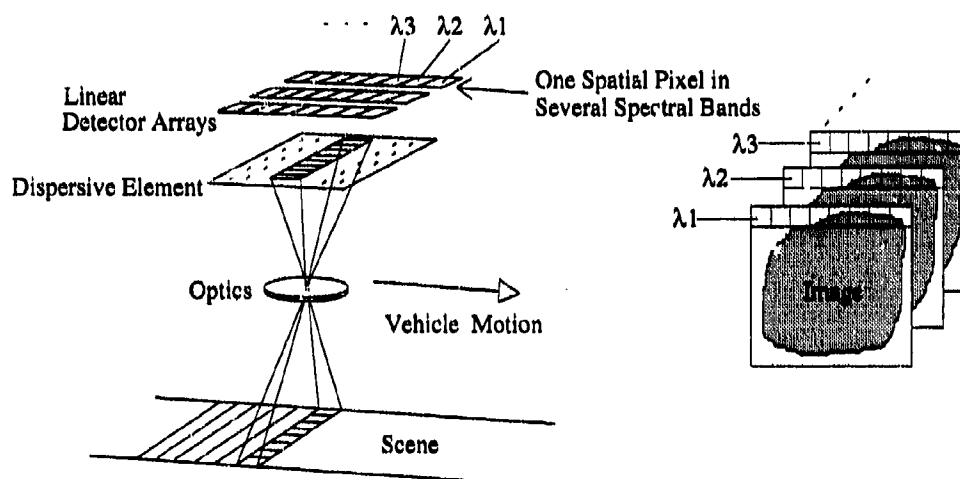


Figure 3. Pushbroom Scanning to Form a Multispectral Image

to several columns of detectors simultaneously by a system of dispersing elements such as prisms or gratings. There is a column of detectors dedicated to each spatial pixel.

Another variation using linear detector arrays is whiskbroom scanning where the linear detector arrays and dispersive element are perpendicular to the pushbroom configuration. The scene is mechanically scanned perpendicular to the vehicle ground track; whiskbroom scanning is used when the desired scene is much wider than one linear array field-of-view.

As stated earlier, staring HI schemes (Figure 4) take advantage of a two-dimensional detector array to gather two-dimensional spatial information with no mechanical scanning for one SFOV. The staring HI system brings about the need for some type of sequential

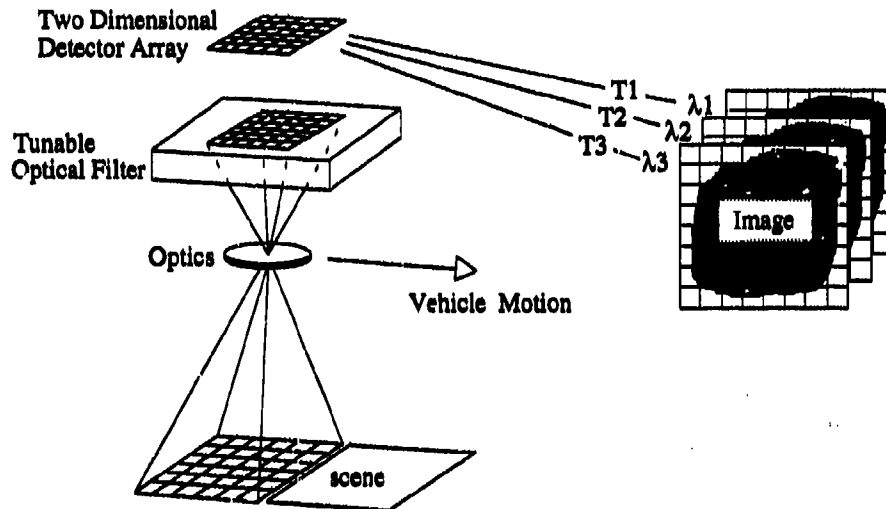


Figure 4. Staring System with Sequential Spectral Information

spectral discrimination method such as a TOF which tunes to  $\lambda_1$  during time  $T_1$ ,  $\lambda_2$  during  $T_2$ , and  $\lambda_3$  during  $T_3$  and so on. Another possibility for sequential spectral discrimination is a rotating filter wheel (Figure 5) that cycles through all of its spectral bands during the time that one SFOV is imaged [5:324]. The filter wheel is tuned mechanically by rotation

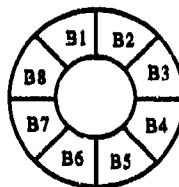


Figure 5. Filter Wheel with Eight Spectral Bands

with one complete revolution per multispectral image. The color wheel approach may work when there are only a few spectral bands but might be impractical for the number of bands required for HI due to the filter wheel size, also mechanical rotation is undesirable in satellite applications.

### Scanning Versus Staring

*Scanning Systems.* HI systems, as discussed in this thesis, fall into two broad categories; scanning systems and staring systems. Almost all of the earth-sensing and environment-sensing satellites use some type of scanning system. A mapping scanning system constructs images of scenes much larger than its SFOV. The resultant image is a continuous long strip of the scene as the vehicle moves forward. Earth remote sensing systems, such as the United States' Landsat system, provide this type of image data [4:473]. The 64 band Moderate Resolution Imaging Spectrometer (MODIS) is a whiskbroom mapping system scheduled to begin operation in the mid-1990's as part of the Earth Observing System (EOS) [6:43], [7:145].

A target-tracking scanning system images a much smaller object or scene. To track one target, the scanning HI system must continually point at the scene using a gimbaled mount. The parent vehicle must make repeated passes over the target. The 32 band NASA Advanced Solid-State Array Spectroradiometer (ASAS) test program used a combination of gimbaled mount and repeated passes to gather object data [8:3-4].

Almost all modern scanning HI systems take spectral data in parallel. In particular, pushbroom scanning finds use in many remote sensing applications such as NASA's proposed High Resolution Imaging Spectrometer (HIRIS) [6:39], [9:136], Europe's Medium Resolution Imaging Spectrometer (MERIS) [10:102] and the Multispectral Scanner System (MSS) in Landsat [4:473].



*Staring Systems.* The staring system proposed by Rees in his remote sensing text would gather spectral information one spectral band at a time for each SFOV; with modern detector array technology, the staring system concept appears to be a promising HI system of the future [11:95-97]. As mentioned earlier, a mechanically tuned filter wheel could provide spectral discrimination for a staring system with a small number of spectral bands. The Japanese plan to use a staring system with filter-wheel spectral discrimination on their eight band Advanced Earth Observing Satellite (ADEOS) [12:196].

*A Comparison.* An advantage of a staring system lies in the amount of radiant energy each detector can gather from one IFOV in one spectral band. Radiant energy is a crucial parameter in HI system operation: generally speaking, more radiant energy is better. Let us go through an admittedly simplified analysis of radiant energy reaching one detector in one spectral band for a pushbroom system versus a staring system. Several assumptions will enable this comparison.

1. The object of interest is square and " $N \times N$ " IFOVs (one SFOV).
2. The object will be imaged in " $L$ " spectral bands.
3. The pushbroom system has " $N$ " linear detector arrays, each  $1 \times L$ . Each linear array images the irradiance from one IFOV into  $L$  spectral bands.
4. The staring system has a single " $N \times N$ " detector array with a tunable optical filter to provide spectral discrimination.
5. The area of the optic for both systems is the same ( $A_0$ ).
6. There are " $T$ " seconds to gather all spatial and spectral information for one SFOV (one complete multispectral image).
7. The irradiance on the optic ( $E_0$ ) from the object is from one SFOV (the object is uniform and lambertian).

With the pushbroom system, the total irradiance on the optic isn't used; the system can only look at one row of IFOVs at a time (the power is divided by " $N$ "). Since there is

one IFOV per linear detector array, the power is divided again by "N". The dispersing element then divides the power due to each IFOV between "L" spectral bands. The integration time for the pushbroom system is the time allowed for one SFOV divided by the number of rows of IFOVs in one SFOV. Radiant energy on one detector, in one band, is the product of power and integration time:

$$Q_{d(SCANNING)} = \frac{E_0 A_0 T}{N^2 L N} = \frac{E_0 A_0 T}{N^3 L} \quad (1)$$

Now let us look at the "L" channel staring system. Remember, we are allowed "T" seconds to gather all spectral and spatial information for one SFOV: the staring system must gather "L" spectral bands in "T" seconds from  $N^2$  IFOVs simultaneously. Radiant energy in the staring case is simply the product of power and integration time [7: 14], or

$$Q_{d(STARING)} = \frac{E_0 A_0 T}{N^2 L} = \frac{E_0 A_0 T}{N^2 L} \quad (2)$$

The last two results show a significant advantage for the staring system in this oversimplified case. In reality, there would be many more losses for both types of systems such as losses in the gratings or optical filters, and losses in the optical train.

#### The Representative HI System and the Ideal Filter

*The Representative HI Systems.* There are a myriad of HI systems in operation and on the drawing board. The HIRIS, proposed as part of the EOS, represents the state-of-the-art in number of spectral channels and channel bandwidth for HI systems. The spectral range of 0.4 to 2.5  $\mu\text{m}$  is imaged in 192 spectral channels simultaneously, FWHM bandwidths range from 10 nm to 50 nm [9]. The HIRIS is meant to provide high spectral

and spatial resolution (IFOV of 30 m<sup>2</sup>) to image relatively small areas; it is not meant to map large areas like the MODIS described next.

The MODIS, also part of the EOS, consists of two sensors MODIS-N and MODIS-T capable of two-day global satellite coverage [7]. The MODIS-T, with tiltable field-of-view, has spectral coverage from 400 to 1040 nm in 64 spectral bands with spectral bandwidth of 10 nm. The MODIS-N has 40 channels with spectral coverage between 470 nm and 14.2  $\mu$ m. Channel bandwidth ranges from 10 nm in the visible region to as much as 500 nm in some of the infrared channels. Although there are many variations, the MODIS-N represents the state-of-the-art in multispectral imaging systems with infrared capabilities fairly well.

*The Ideal TOF for Spectral Discrimination in HI Applications.* This thesis defines the ideal TOF by assuming the TOF would provide spectral discrimination for a HIRIS-type instrument in the visible through near infrared region (400 nm - 3.0  $\mu$ m) and for a MODIS-N-like system in the infrared region (3.0  $\mu$ m - 5  $\mu$ m, 7  $\mu$ m - 14.2  $\mu$ m). The ideal TOF has 100% transmission in the pass band, 100 % rejection out of the pass band, a 10 nm bandwidth in the visible region (400 nm - 1.1  $\mu$ m), a 20 nm bandwidth in the near infrared (1.1  $\mu$ m - 3.0  $\mu$ m), a 50 nm bandwidth in the middle infrared (3.0  $\mu$ m - 5.0  $\mu$ m), and a 300 nm bandwidth in the far infrared (7  $\mu$ m - 14.2  $\mu$ m). Ideally one TOF would tune over the whole spectrum of interest (400 nm - 14.2  $\mu$ m). This thesis did not address such filter parameters as filter field-of-view, losses due to reflection or absorption, channel selection speed, filter power requirements, or other material considerations such as temperature dependence.

### Methodology

The investigation into HI was primarily a search through the scientific literature concerning HI systems and NASA's technical documentation of the EOS. HI system

spectral discrimination requirements used in this thesis are quite general and were deduced from technical specifications for the MODIS and HIRIS sensors scheduled to be part of EOS. HI system spectral discrimination requirements were then translated into ideal TOF characteristics; this thesis uses the ideal TOF characteristics for comparison purposes. Scientific literature and patents yielded the information concerning existing filters and tuning methods with some modifications introduced during the analysis of certain filters.

The combination of analytical and computer numerical analysis helped provide insight into filtering and tuning methods. Analytical expressions are presented whenever possible for filtering and tuning methods; some expressions are taken from the literature while others were derived. Jones Calculus and numerical software provide simulations for all filters and filter combinations considered in this thesis [14]. The comparison between the computer filter simulations and the "ideal" filter are the basis for the conclusions about each filter's applicability to HI.

Materials analysis is only cursory; this thesis is not a study of birefringent or polarizer materials. Tuning methods such as electro-optic tuning and electrically rotated optic axis tuning are based on phenomenon that certain materials exhibit; however, no specific material parameters were used in the computer simulations.

### Assumptions and Limitations

Several assumptions are made to limit this work to fundamental filtering concepts and filter tuning considerations. First, this thesis ignores most real-world detector constraints including detector spectral response. The filter investigations assume ideal lossless waveplates, achromatic waveplates whose optic axis is electrically rotatable, and non-dispersive electro-optic birefringent materials which are capable of any combination of indices of refraction and crystal thickness desired. Losses due to reflection and refraction are also ignored. The above assumptions greatly simplify the filter and tuning analysis and

detract little from the value of the results at this stage. Also, the results are more tractable and easily understood.

## II. Lyot Based Filters

### Introduction

The findings for the Lyot based TOFs investigated as part of this thesis are presented in this chapter. Where possible, analytic expressions are presented to define each filter's characteristics, to include: filter transmission versus wavelength, bandwidth, and tuning range. Analytic expressions provide verification of the computer simulations which yield information about certain filters for which no analytic expression was available. It should be noted once more that many practical considerations such as absorption loss, reflection loss, birefringent element thicknesses, and material acceptance angle are neglected to keep the analytical expressions and computer simulations tractable.

### The Lyot Birefringent Filter

*The Single Stage Lyot Filter.* Lyot invented the birefringent filter in 1933 to use in solar research [1]. A single stage Lyot filter consists of a piece of birefringent material (usually uniaxial) positioned between two parallel or crossed polarizers (Figure 6). The elements are stacked with faces parallel to each other; the optic axis of the birefringent element is parallel to the faces of the other filter elements and at an angle " $\rho$ " to the extinction axis of the input polarizer.

The input polarizer in Figure 6 converts the incoming light to linearly polarized light in the "Y" direction. If the incoming light is randomly polarized, 50 percent of the incoming light is lost through the input polarizer. The linearly polarized light is broken into two components (Eigen polarizations), one component polarized along the fast axis of the birefringent plate and the other along the slow axis. Each component propagates through the birefringent plate at a different velocity causing a phase difference to develop between the two. The amount of phase difference, along with the relative magnitude of the Eigen components and the angle " $\rho$ ", determine the type of polarization out of the

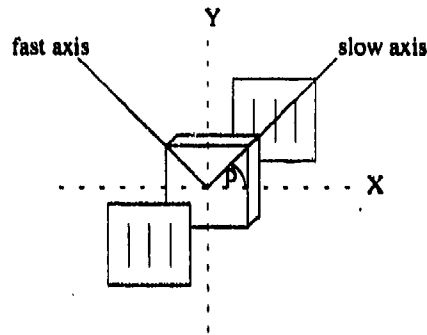


Figure 6. A Single Lyot Filter Element

birefringent plate. Hecht gives the following equation to describe the resulting polarization of two orthogonal optical disturbances which are out of phase with one another by the phase difference " $\epsilon$ " [15:273].

$$\left( \frac{E_y}{E_{oy}} \right)^2 + \left( \frac{E_x}{E_{ox}} \right)^2 - \left( \frac{E_y}{E_{oy}} \right) \left( \frac{E_x}{E_{ox}} \right) \cos \epsilon = \sin^2 \epsilon \quad (3)$$

where

$$E_x = E_{ox} \cos(kz - \omega t), \quad E_y = E_{oy} \cos(kz - \omega t + \epsilon) \quad (4)$$

and

$$\epsilon(\nu) = \frac{2\pi\nu\Delta n d}{c} \quad (5)$$

where  $\Delta n$  is the difference between the slow and fast indices of refraction in the birefringent material,  $\nu$  is the frequency,  $d$  is the thickness of the material, and  $c$  is the speed of light in free space. Equation (5) describes an ellipse making an angle " $\alpha$ " with the  $(E_x, E_y)$  coordinate system as shown in Figure 7; the  $(E_x, E_y)$  coordinate system is defined by the fast and slow axes of the birefringent plate and  $E_{ox}$  and  $E_{oy}$  are field magnitudes.

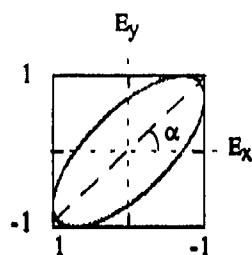


Figure 7. Plot Showing Elliptical Polarization

Hecht gives the equation for  $\alpha$  as [15:273]:

$$\tan 2\alpha = \frac{2E_{ox}E_{oy}\cos\epsilon}{E_{ox}^2 - E_{oy}^2} \quad (6)$$

One can make some interesting deductions from Equation (6). First, when  $E_{ox}$  and  $E_{oy}$  are equal in magnitude ( $\rho = \pm \pi/4$ ),  $\alpha$  can only be  $\pm \pi/4$ , and when  $\epsilon = \pm \pi/2$   $\alpha$  is zero. The Lyot geometry is when the magnitudes of  $E_x$  and  $E_y$  are equal ( $\rho = \pi/4$ ). Polarization plots for the two waves after they exit the birefringent plate for various values of  $\epsilon$  are in Figure 8. We see that with no plate between the polarizers ( $\epsilon = 0$ ), the

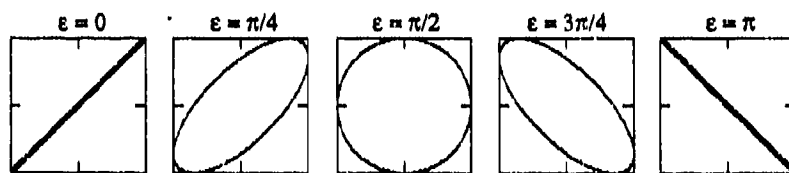


Figure 8. Polarization Plots with  $E_{ox} = E_{oy}$  for Various Values of  $\epsilon$

polarization is linear and at an angle of  $\pi/4$  to  $E_x$  (parallel to the transmission axis of the input polarizer). As  $\epsilon$  is increased from 0 to  $\pi/2$  we see the ellipse that describes the polarization get "wider" until at  $\epsilon = \pi/2$  the polarization is circular. As  $\epsilon$  further increases from  $\pi/2$  to  $\pi$ , we see the polarization go from circular to elliptical again only



the orientation of the ellipse is at an angle of  $-\pi/4$  to the  $E_x$  axis (perpendicular to the input polarizer) and finally at  $\epsilon = \pi$  the polarization is again linear. For a fixed angle "p" the polarization out of the birefringent plate is determined by the amount of phase difference between the two Eigen components; thus, the intensity of light transmitted by the output polarizer depends on the phase difference introduced by the birefringent plate. Recall that the phase difference (retardance) introduced by a birefringent material depends on the frequency of the light impinging on the material (Equation 5). The filtering action comes about because of this dependence of retardance on frequency. A sample plot of the transmission spectrum for a single stage Lyot filter is shown in Figure 9. As the plot in

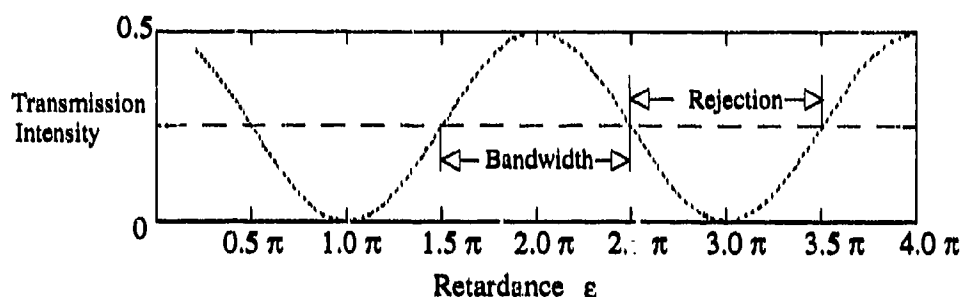


Figure 9. Transmission Spectrum for a One Stage, Parallel Polarizer, Lyot Filter

Figure 9 shows, the transmission spectrum of a one stage Lyot filter is periodic with transmission peaks where  $\epsilon$  is a multiple of  $2\pi$  and transmission minimums occur at odd multiples of  $\pi$ . The half power points are when the retardance is an odd multiple of  $\pi/2$  which corresponds to circular polarization. Circular polarization can be decomposed into two equal orthogonal linear polarizations; one is passed by the output polarizer while the other is totally extinguished. The analytic expression given by Yariv for the one stage Lyot filter with parallel polarizers is [16:130]:

$$T = \frac{1}{2} \cos^2 \left( \frac{\epsilon}{2} \right) \quad (7)$$

In Equation (7) it is assumed that the polarizers are ideal and the incoming light has polarization such that half the incoming power is lost through the first polarizer.

*The Multiple Stage Lyot Filter.* A one stage Lyot filter is not very useful because the bandwidth is the same as the rejection region. To narrow the bandwidth,  $\epsilon$  can be increased but this decreases the rejection region correspondingly. The most effective way to narrow the bandwidth is to add more stages to the filter such that the spectrum of each added stage increases the rejection region and decreases the bandwidth. A two stage Lyot geometry is shown in Figure 10. In each successive added stage, the thickness of

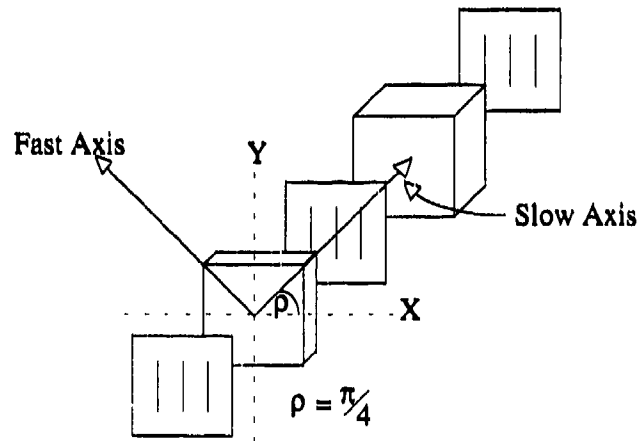


Figure 10. A Two Stage Lyot Filter

the birefringent plate doubles from that of the previous stage; the transmission spectrum of each successive stage has a spectral period of one half that of the previous stage. When two stages are cascaded, the transmission spectra of each stage effectively multiply together as shown in Figure 11. In general, adding stages narrows the bandwidth and widens the rejection region of the filter.

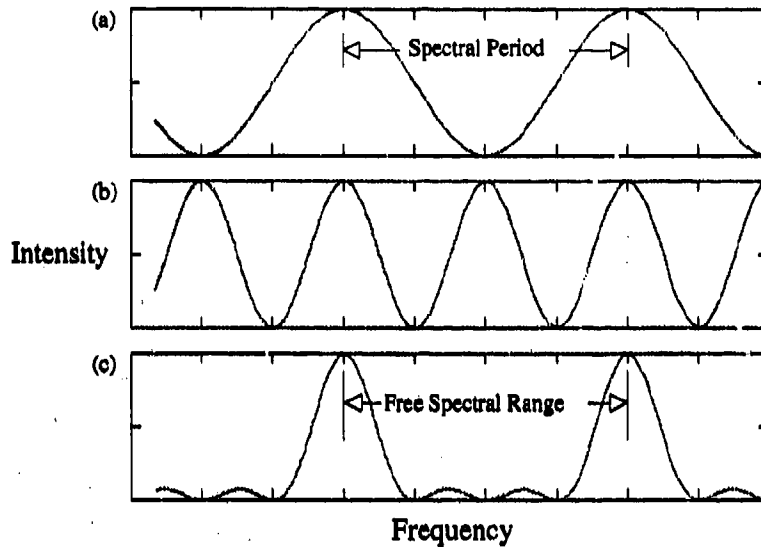


Figure 11. Transmission vs. Frequency for (a) The First Stage of a Lyot (b) The Second Stage of a Lyot (c) The Two Stages Cascaded Together (Two Stage Lyot Filter)

The general relationship for an N-stage Lyot filter is simply the product of the transmission functions for individual stages (Equation 7). This is shown in Equation 8:

$$T = \frac{1}{2} \prod_{i=1}^N \cos^2 \left( \frac{2^{N-i} \epsilon}{2} \right) \quad (8)$$

The full-width-half-maximum (FWHM) bandwidth of the multistage Lyot can be estimated by the bandwidth of the final stage as long as N isn't too large. The equation below gives the bandwidth of the final (thickest) stage;

$$BW_{Hz} = \frac{c}{\Delta n d_1 2^N} \quad \text{or} \quad BW_{\lambda} = -\frac{\lambda_0^2}{\Delta n d_1 2^N} \quad (11)$$

where the thinnest stage thickness is  $d_1$  and  $\lambda_0$  is the center wavelength of the passband of interest.

While the thickest element determines the bandwidth of the Lyot filter, the thinnest element determines the free spectral range. The expression for free spectral range is the same expression as for the bandwidth only we use the thickness of the thinnest stage.

$$\text{FSR} = \frac{c}{\Delta n d_1} \quad (\text{in frequency}) \quad (10)$$

Equations 9 and 10 show that a large  $\Delta n d_1$  product helps to narrow the bandwidth; unfortunately, the free spectral range is decreased as well. In a filter design where both large free spectral range and narrow bandwidth are important, the free spectral range must be set first by choosing the correct  $\Delta n d_1$  product; then the bandwidth can be achieved by choosing the proper number of stages.

*Transmission profile of the Lyot Filter.* Although the Lyot filter is treated like a bandpass filter in this thesis, it is not truly a bandpass filter in that it has more than one pass band. The center frequencies for the multiple pass bands are found by looking at the transmission function of Equation 8 and the expression for retardance in Equation 5. Transmission peaks occur when:

$$v = \frac{kc}{\Delta n d_1} \quad \text{or} \quad \lambda = \frac{\Delta n d_1}{k} \quad k = 0, 1, 2, 3, \dots \quad (11)$$

The transmission profile of the Lyot filter is not rectangular as we would like and the transmission and rejection are not unity and zero respectively. Fifty percent of randomly polarized input intensity is lost at the input polarizer, so even a filter with ideal elements is limited to 50 percent transmission. In the rejection region, we see in Figure 11 that the side lobes of the transmission band are substantial (usually around five percent of the main lobe). A section later in this chapter deals with side lobe suppression.

### The $\Delta n$ -tuned Lyot Filter

***Tuning Mechanism.*** The standard Lyot filter provides the basis for understanding the tunable Lyot filter. In the  $\Delta n$ -tuned Lyot case, the birefringent element thicknesses are constant but the birefringence ( $\Delta n$ ) of the material is variable. An electric field applied to certain materials changes  $\Delta n$  in the material. It has been shown that under certain conditions a relationship exists between the applied dc field (strength and direction) and the birefringence exhibited by the material [16:220]. In the present study, no specific material is used and it is assumed that any range of  $\Delta n$  is possible and that  $\Delta n$  can be changed without affecting the Eigen directions in the material.

***Tuning Characteristics.*** "Tuning" refers to movement of the center frequency (or wavelength) by changing some parameter of the filter. A multistage Lyot filter with fixed birefringent element thicknesses can be tuned by changing  $\Delta n$  in the birefringent material for each stage simultaneously in the same fashion. A look at Equations 9 and 11 shows us that for any particular pass band, the bandwidth and center frequency are inversely proportional to  $\Delta n$ . In other words, a reduction of  $\Delta n$  moves any particular pass band up in frequency while the bandwidth (in Hz) of that pass band gets narrower. Tuning range is defined as the maximum frequency or wavelength range over which the pass band of interest can be moved while maintaining only one pass band in the frequency or wavelength range of interest. From Figure 11 we deduce that the tuning range must be less than the free spectral range given by Equation 10. If the filter is tuned over a frequency range equal to or larger than one free spectral range, there can be more than one passband in the frequency range of interest. The next section illustrates the tuning characteristics of the  $\Delta n$ -tuned Lyot filter with examples of HI system applications.

***Operation in the HI spectral region.*** In this section, filter characteristics are expressed in terms of wavelength because HI system requirements are usually expressed in wavelength units. The spectral range of interest for HI applications is 400 nm to 14.2  $\mu\text{m}$

in terms of free space wavelength, or using the fact that frequency is the speed of light divided by the free space wavelength, 21.1 terahertz (THz) to 750 THz in terms of frequency. The product of the thickness of the thinnest plate and the material birefringence ( $\Delta n$ ) determines both where the transmission peaks will be and the free spectral range between the transmission peaks. For HI spectral discrimination we want a large free spectral range and the ability to tune to any wavelength of interest. If we choose the product of  $\Delta n d_1$  such that the first transmission peak ( $k = 1$ ) is at 400 nm then the passband center wavelength is moved to longer wavelengths by increasing  $\Delta n$  (assuming constant plate thickness) and we have tunability. A doubling of  $\Delta n$  moves the center wavelength from 400 nm to 800 nm; but, along with the peak at 800 nm ( $k = 1$ ) is another peak at 400 nm ( $k = 2$ ). This means that if we start tuning at 400 nm we can only tune to some wavelength slightly less than twice 400 nm before a second transmission peak begins to appear; in general the tuning range for the  $\Delta n$ -tuned Lyot filter is a little less than the filter's shortest wavelength. In terms of wavelength this filter is ideally capable of tuning from 400 nm to slightly less than 800 nm in the visible, the entire mid-infrared (3  $\mu\text{m}$  - 5  $\mu\text{m}$ ) and most of the far infrared (7  $\mu\text{m}$  to slightly less than 14  $\mu\text{m}$ ).

As eluded to above, bandwidth (expressed in wavelength units) of a particular transmission peak does not stay constant over the filter tuning range. In fact, bandwidth changes linearly with center wavelength for the  $\Delta n$ -tuned Lyot filter. In the visible case, if we set the number of stages such that the bandwidth is 10 nm at a center wavelength of 400 nm, then tune the filter to 800 nm and recalculate the bandwidth, we see that the bandwidth expressed in terms of wavelength doubles when the center wavelength doubles. The results of a computer simulation are shown below in Figure 12. Notice the second pass band at 400 nm when the filter is tuned all the way to 800 nm. Actual tuning range in the visible spectral region would be slightly less to keep the second pass band out of the spectral range of interest.

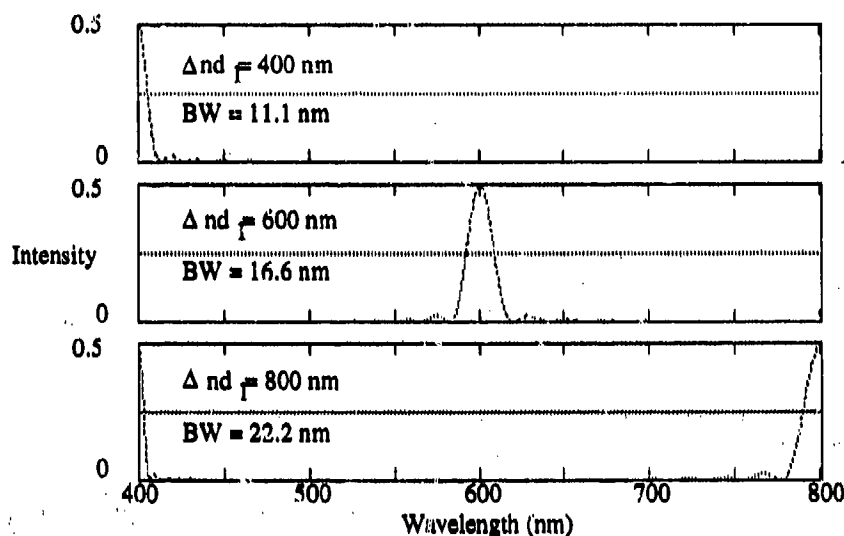


Figure 12. Tuning Characteristics for a 5-stage  $\Delta n$ -tuned Lyot Filter in the Visible Region

Another important characteristic of a filter for HI application is the number of spectral bands it can support without the bands interfering with each other. If each pass band is only allowed to overlap as far as its half power points with its neighbor's half power points, then the number of channels is the number of pass bands which fit in the tuning range in this manner. As an example, the channels were calculated numerically for the five stage  $\Delta n$ -tuned Lyot discussed above. A possible channel allocation solution is presented in Table 1; about 25 channels are possible from 400 to 800 nm. Note that an additional stage added to this filter halves the bandwidth of any particular passband and thereby doubles the number of channels possible.

It is obvious that a single  $\Delta n$ -tuned Lyot filter cannot cover the whole HI spectrum. In fact, 5 such filters are required to tune over the HI spectrum. Table 3 shows one possible set of  $\Delta n$ -tuned Lyot filters for the HI spectrum; notice that the total number of channels exceeds 200.

**Table 1. Example of Channel Allocation for a  $\Delta n$ -tuned Lyot Filter in the Visible Region**

Channel	Pass Band Center Wavelength (nm)
1	400.0
2	411.2
3	422.8
4	434.8
5	446.8
6	459.6
7	472.4
8	485.6
9	499.2
10	513.2
11	527.6
12	542.4
13	557.6
14	573.2
15	589.6
16	606.0
17	623.2
18	640.4
19	658.4
20	677.2
21	695.6
22	715.2
23	735.2
24	756.0
25	777.2

**Table 2. A Set of  $\Delta n$ -tuned Lyot Filters Required to Tune Over the HI Spectrum**

Tuning Range	Number of Stages	Bandwidth Range (nm)	Maximum Channels
400 nm - 800 nm	6	5.6 - 11.2	50
800 nm - 1.6 $\mu\text{m}$	6	11.2 - 22.4	50
1.6 $\mu\text{m}$ - 3.0 $\mu\text{m}$	6	22.4 - 41.6	44
3.0 $\mu\text{m}$ - 5.0 $\mu\text{m}$	6	41.6 - 68.6	36
7.0 $\mu\text{m}$ - 14.0 $\mu\text{m}$	5	194 - 288	25



### The Wave-Plate-Tuned Lyot Filter

*Tuning Mechanism.* An alternate method of changing the passband center frequency was suggested by Title and Rosenberg [17]. This method uses an achromatic quarter-wave plate, and a rotatable achromatic half-wave plate as shown in Figure 13. Sharp and

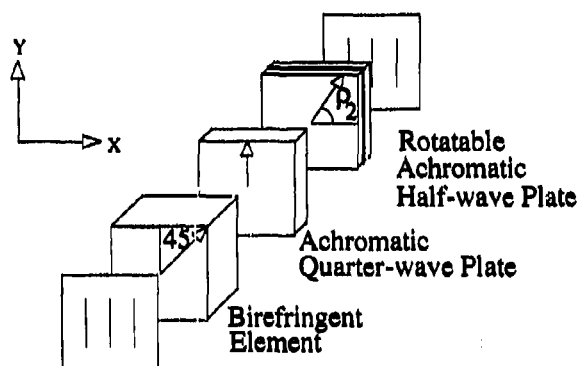


Figure 13. One Stage Lyot Filter Tuned with Achromatic Wave Plates

others demonstrated a single stage filter of this type using a special liquid crystal electrically rotated wave plate [18].

The polarization out of the birefringent plate is in general elliptical (Figure 8). The achromatic quarter-wave plate converts elliptical polarization to linear polarization; the angle that the linear polarization makes with the X axis depends on the amount of retardance of the birefringent element. If the birefringent plate thickness and  $\Delta n$  are held constant, the retardance is inversely proportional to signal wavelength. Thus, the angle of the linear polarization coming out of the quarter-wave plate depends on the wavelength. The half-wave plate changes the sign of the angle between the input wave's polarization vector and the fast or slow axis of the crystal (Figure 14); thus, the half-wave plate can be rotated such that the resulting polarization matches that of the output polarizer.

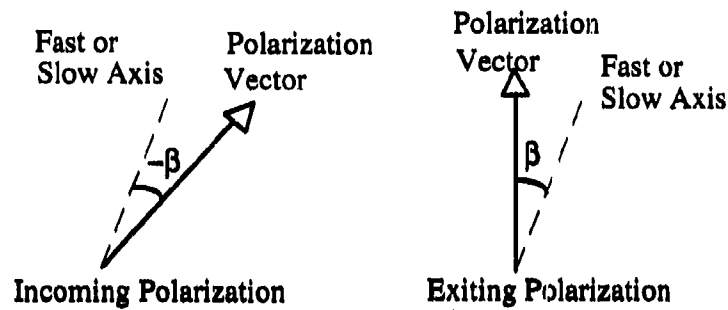


Figure 14. Linear Polarization Angle Change Through a Half-wave Plate

**Tuning Characteristics.** Using Jones calculus, the transmission of a one stage Lyot filter with rotatable half-wave plate tuning can be calculated. The Y-polarized transmission function is:

$$T_{1 \text{ stage}} = \frac{1}{4} \sin(\epsilon) \sin(4\rho_2) - \frac{1}{2} \cos(\epsilon) \sin^2(2\rho_2) + \frac{1}{2} \cos^2\left(\frac{\epsilon}{2}\right) \quad (14)$$

where  $\epsilon$  is given by Equation 5, and  $\rho_2$  is the angle between the X axis and the fast or slow axis of the rotatable plate (Figure 13).

To apply this result to a multi-stage filter we must remember that the retardance of each successive stage is twice that of the previous stage because the thickness of the birefringent plates double with each stage. Since the angle of the linear polarization out of the quarter-wave plate is proportional to the retardance of the birefringent plate immediately before it, the half-wave plate rotation angle for each successive stage must also be twice that of the previous stage. Taking the product of the transmission functions (Equation 12 with correct thickness) for each of "N" stages and correcting appropriately for the doubling of the half-wave plate rotation angles we get:

$$T = \frac{1}{2} \prod_1^N \left[ \frac{1}{2} \sin(2^{N-1} \epsilon) \sin(2^{N+1} \rho_2) - \cos(2^{N-1} \epsilon) \sin^2(2^N \rho_2) + \cos^2(2^{N-2} \epsilon) \right] \quad (13)$$

Notice that when  $\rho_2$  is an integer multiple of  $\pi/2$  Equation 13 becomes the same as Equation 8 for the standard Lyot.

The FWHM bandwidth is closely approximated by the bandwidth of the last stage and is given by Equation 9, the same as the standard Lyot. Even though Equation 9 expresses the bandwidth, unlike the standard Lyot  $\Delta n d$  does not change when the filter is tuned so the bandwidth remains constant (in frequency) throughout the tuning range which means bandwidth expressed in wavelength units grows quadratically with wavelength. Like the standard Lyot the bandwidth is still narrowed by addition of stages.

Tuning range for this filter begins at  $\lambda = \Delta n d_1$  for  $\rho_2 = \pi/2$  and continues toward longer wavelengths as  $\rho_2$  is decreased;  $\lambda$  approaches infinity as  $\rho_2$  approaches zero. In this case maximum tuning range must be expressed in frequency and is given by:

$$TR = \frac{c}{\Delta n d_1} \quad (14)$$

*Operation in the HI Spectral Region.* The HI system requirements specify a 10 nm bandwidth for the 400 nm to 1.1  $\mu\text{m}$  spectral region, a 20 nm bandwidth for the 1.1  $\mu\text{m}$  to 3  $\mu\text{m}$  region, a 50 nm bandwidth for the 3  $\mu\text{m}$  to 5  $\mu\text{m}$  region, and a 300 nm bandwidth for the 7  $\mu\text{m}$  to 14.2  $\mu\text{m}$  region. Unlike the  $\Delta n$ -tuned Lyot, the wave-plate-tuned Lyot is capable of any of these tuning ranges or capable of tuning over more than one with a single filter. The maximum number of channels is easy to calculate; since the bandwidth is constant in frequency, the desired tuning range (expressed in frequency for this calculation) is simply divided by the bandwidth in frequency to yield the maximum number of channels. For the  $\Delta n$ -tuned Lyot the bandwidth in frequency actually decreased with increasing channel frequency; thus, for a given number of stages and element thicknesses the wave-plate-tuned filter will support fewer channels per given tuning range.

A 5-stage filter has an 11.2 nm bandwidth for a pass band centered at 400 nm; as it is tuned from 400 nm toward longer wavelengths to 800 nm, the bandwidth quadruples to 44.8 nm. The number of channels for this filter is 16 compared with 25 for the  $\Delta n$ -tuned filter with the same birefringent elements. Figure 15 shows computer generated tuning

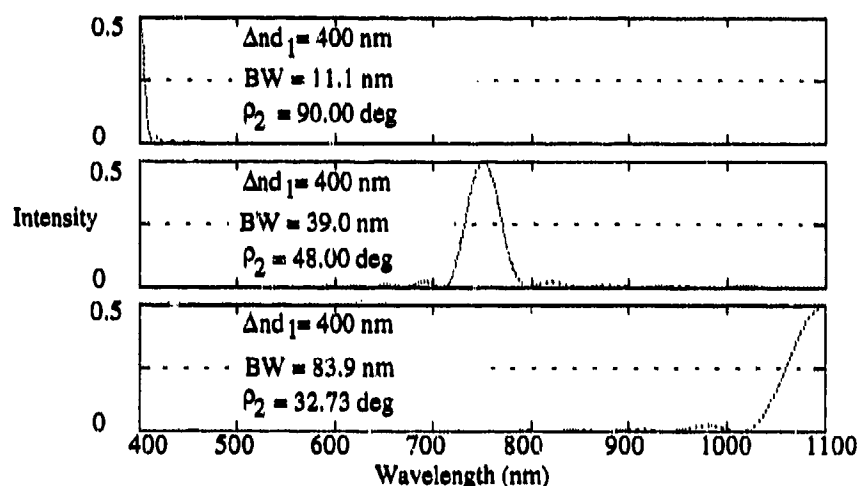


Figure 15. Tuning Characteristics for a 5-stage Wave-plate-tuned Lyot Filter in the Visible to Near-infrared Region

characteristics for a 5-stage wave-plate-tuned Lyot filter in the visible to near-infrared region. Table 3 shows a set of wave-plate-tuned Lyot filters that could tune over the HI spectrum.

Table 3. A Set of Wave-plate-tuned Lyot Filters Required to Tune Over the HI Spectrum

Tuning Range	Number of Stages	$\Delta n_1$ Product	Bandwidth Range (nm)	Maximum Channels
400 nm - 1.1 $\mu$ m	6	400 nm	5.6 - 42.4	46
1.1 $\mu$ m - 3.0 $\mu$ m	6	1.1 $\mu$ m	15.2 - 113.2	46
3.0 $\mu$ m - 5.0 $\mu$ m	6	3.0 $\mu$ m	41.5 - 115.3	30
7.0 $\mu$ m - 14.2 $\mu$ m	6	7.0 $\mu$ m	96.9 - 398.8	36

Both Figure 15 and Table 3 bear out the major disadvantage of the wave-plate-tuned Lyot filter, its quadratic bandwidth growth as it is tuned to longer wavelengths. This filter also needs 3 times as many elements compared with the  $\Delta n$ -tuned Lyot filter.

#### Pass Band Shaping with Lyot Type Filters

*The Contrast Element.* A contrast element is used to suppress pass band side lobes in the transmission profile [17]. The contrast element consists of another Lyot stage whose thickness is close to that of the second to the last stage. Computer generated plots of a standard 5-stage Lyot and a 5-stage Lyot with a contrast element appear in Figure 16. The logarithmic scale allows us to see about a 5-fold decrease in the main side lobes. Both  $\Delta n$ -tuning and wave-plate-tuning work with this filter as we would expect.

*Non-standard Plate Thickness.* The non-standard plate thickness Lyot filter differs from the standard Lyot filter only in the thickness relationship between the birefringent plates. Each successive plate thickness is an integer multiple of the thinnest plate; but there can be no common factor between any of the multipliers except 1 [19]. Many

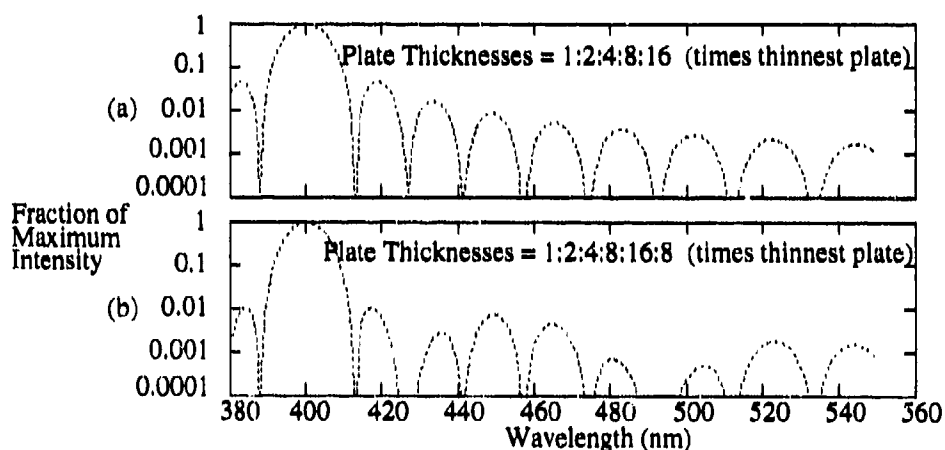


Figure 16. Side Lobe Suppression Using a Contrast Element (a) 5-stage Lyot Filter with No Contrast Element (b) 5-stage Lyot Plus a Contrast Element (6 stages total)

thickness combination possibilities exist. By computer experimentation it was found that a narrower bandwidth could be achieved at the expense of additional side lobes by making the thickness of the thickest element greater than that of a Lyot with the same number of stages. Figure 17 shows both a standard 5-stage Lyot filter profile and a 5-stage non-standard plate thickness filter profile. The non-standard filter bandwidth is narrower at the

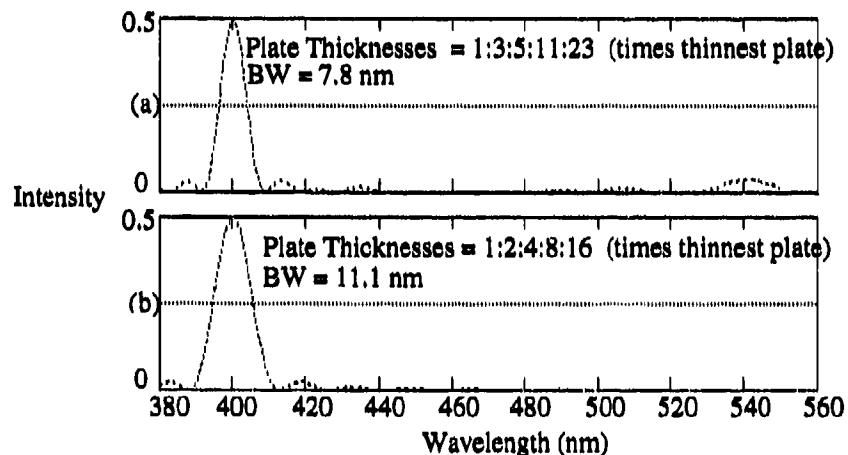


Figure 17. Spectral Profile for (a) 5-stage Lyot Filter Non-standard Plate Thicknesses  
(b) Standard 5-stage Lyot

expense of extra substantial side lobes away from the pass band. This filter lends itself to  $\Delta n$ -tuning in the same manner as the standard Lyot. Wave-plate-tuning works as well; however, the angle of wave plate rotation of all but the thinnest stage will be a multiple of the rotation for the thinnest stage. The multiplier for a given stage is the same as the thickness multiplier. The filter in Figure 17a tuned in this manner has a bandwidth of 7.8 nm for a 400 nm pass band and a 59 nm bandwidth when tuned to a 1.1  $\mu\text{m}$  and will support 32 channels.

*Arbitrary Pass Band Shapes.* There are at least two methods for synthesizing arbitrary pass band shapes using Lyot-type filter elements. Ammann and Chang describe

one method which tends to use a large number of Lyot elements [20]. The theoretical transmission of these filters is low and it doesn't offer any improvements in tuning characteristics as far as bandwidth dependence on the pass band wavelength. A second technique was proposed by Title which uses lossy interior polarizers and alternating azimuth angles for the birefringent elements (Figure 18); the entrance and exit polarizers are still perfect polarizers [21]. The lossy polarizer passes all vertically polarized light and

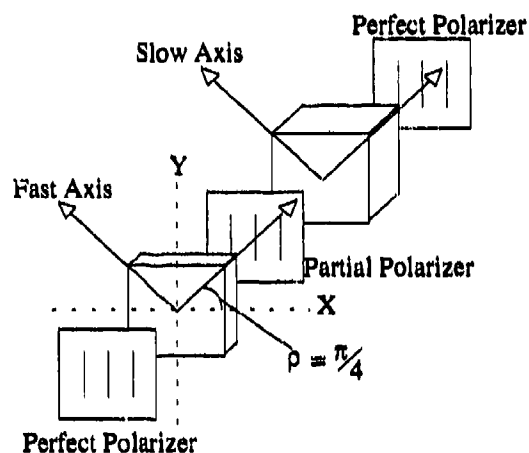


Figure 18. A Two Stage Lyot Filter with Lossy Polarizer

a fraction " $\beta$ " of the horizontally polarized light. A perfect polarizer has  $\beta = 0$  and no polarizer is  $\beta = 1$ ; as  $\beta$  is increased from zero the pass band widens and side lobes decrease. While this technique can improve the passband characteristic (at the cost of more stages) it doesn't offer anything new in the way of tuning or bandwidth control as the filter is tuned.

### III. Solc Based Filters

#### Introduction

The findings for the Solc based TOFs investigated as part of this thesis are presented in this chapter. Where possible, analytic expressions are presented to define each filter's characteristics, to include: filter transmission versus wavelength, bandwidth, and tuning range. Computer simulations provide verification of the analytic expressions and yield information about certain filters for which no analytic expression was available. It should be noted once more that many practical considerations such as absorption loss, reflection loss, birefringent element thicknesses, and material acceptance angle are neglected to keep the analytical expressions and computer simulations tractable. These simplifications do not detract significantly from the optical filtering concepts contained herein.

#### The Solc Birefringent Filter

The Solc filter, named after its inventor, is the second general form of the birefringent filter [2]. The Solc filter consists of a stack of identical birefringent plates between two polarizers. The plates have their fast and slow axis in the same plane as the face of each crystal and the fast or slow axis of each plate is at a prescribed angle (azimuth angle) with the transmission axis of the input polarizer. There are two main variations of the standard Solc geometry, the folded Solc (Figure 19a) and the fan Solc (Figure 19b). In the folded Solc configuration, the azimuth angles of each plate alternate between  $\rho$  and  $-\rho$  and the output polarizer is perpendicular with the input polarizer. In the fan configuration the angles are  $\rho, 3\rho, 5\rho, 7\rho$ , etc.

The azimuth angle for an "N" plate folded or fan Solc filter is given in [16:135] by:

$$\rho = \frac{\pi}{4N} \quad (15)$$



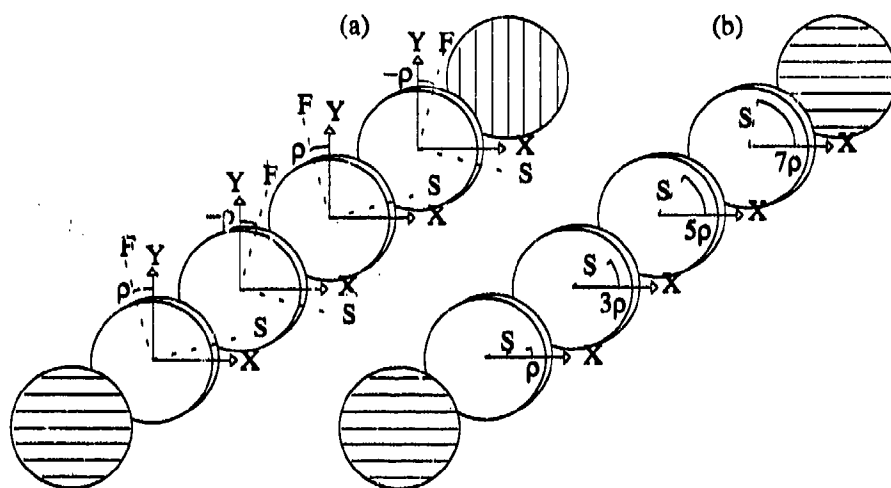


Figure 19. (a) A 4-stage Folded Solc Filter (b) A 4-stage Fan Solc Filter

Using Jones' calculus and assuming the input polarization is parallel to the transmission axis of the input polarizer, Yariv derived an expression for the intensity transmission of the N-stage folded Solc filter by first writing the resultant matrix of all the birefringent plates as [16:135]:

$$M = \begin{pmatrix} A & B \\ C & D \end{pmatrix}^m \quad (16)$$

where  $N = 2m$  ( $N$  is assumed even for mathematical convenience). The expressions for the elements of  $M$  are:

$$\begin{aligned} A &= (\cos \frac{1}{2} \epsilon - j \cos 2\rho \sin \frac{1}{2} \epsilon)^2 + \sin^2 2\rho \sin^2 \frac{1}{2} \epsilon \\ B &= \sin 4\rho \sin^2 \frac{1}{2} \epsilon \\ C &= -B \\ D &= (\cos \frac{1}{2} \epsilon + j \cos 2\rho \sin \frac{1}{2} \epsilon)^2 + \sin^2 2\rho \sin^2 \frac{1}{2} \epsilon \end{aligned} \quad (17)$$

where

$$\varepsilon = \frac{2\pi\Delta n d}{\lambda} \quad (\text{retardance of one plate}) \quad (18)$$

Next, using Chebyshev's identity a closed form for  $M$  is derived.

$$M = \begin{pmatrix} \frac{A \sin[m \cos^{-1}[\frac{1}{2}(A+D)]] - \sin[(m-1) \cos^{-1}[\frac{1}{2}(A+D)]]}{\sin[\cos^{-1}[\frac{1}{2}(A+D)]]} & \frac{B \sin[m \cos^{-1}[\frac{1}{2}(A+D)]]}{\sin[\cos^{-1}[\frac{1}{2}(A+D)]]} \\ \frac{C \sin[m \cos^{-1}[\frac{1}{2}(A+D)]]}{\sin[\cos^{-1}[\frac{1}{2}(A+D)]]} & \frac{D \sin[m \cos^{-1}[\frac{1}{2}(A+D)]] - \sin[(m-1) \cos^{-1}[\frac{1}{2}(A+D)]]}{\sin[\cos^{-1}[\frac{1}{2}(A+D)]]} \end{pmatrix} \quad (19)$$

Finally, the X-polarized field intensity of the emerging beam for a folded Solc filter is given by:

$$T_{\text{folded}} = |M_{21}|^2 = \left| \tan 2\rho \cos \chi \frac{\sin N\chi}{\sin \chi} \right|^2 \quad \text{where} \quad \left( \cos \chi = \cos 2\rho \sin \frac{\varepsilon}{2} \right) \quad (20)$$

Similarly, the Transmissivity for a fan Solc filter is:

$$T_{\text{fan}} = |M_{21}|^2 = \left| \tan 2\rho \cos \chi \frac{\sin N\chi}{\sin \chi} \right|^2 \quad \text{where} \quad \left( \cos \chi = \cos 2\rho \cos \frac{\varepsilon}{2} \right) \quad (21)$$

The picture of how the folded Solc filter works becomes clearer if we let  $\varepsilon = \pi, 3\pi, 5\pi$  etc. (when the plates are half-wave plates). Each half-wave plate rotates incident linear polarization by twice the angle between the incoming polarization and the fast (or slow) axis of the crystal (Figure 20). At those wavelengths where the birefringent plates are half-wave plates, all of the X-polarized incident light is passed through the Y-oriented exit polarizer. The intensity of the output is reduced at other wavelengths; thus, the Solc arrangement is a bandpass filter with multiple pass bands. If  $\lambda = \lambda_0$  is the wavelength where  $\varepsilon = \pi$ , then transmission peaks will occur at  $\lambda_0, \lambda_0/3, \lambda_0/5$ , etc. The widest

spectral distance between transmission peaks is between the  $\lambda_0$  and  $\lambda_0/3$  transmission peaks.

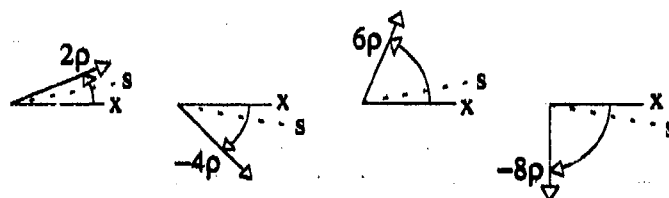


Figure 20. Rotation of the Incoming x-polarized Light After Each Half-wave Plate in a 4-stage Solc Filter

The fan Solc passes wavelengths for which the birefringent plates act as full-wave plates ( $\epsilon = 0, \pi, 2\pi, 4\pi$ , etc.). At these wavelengths the polarization is not rotated and is passed through the exit polarizer; at all other wavelengths the polarization is changed and loss occurs at the exit polarizer. The result is that the spectrum for the fan Solc is the same as that of a folded Solc with plate retardance of  $\epsilon + \pi$ . The widest spectral distance between transmission peaks for the fan Solc is between the  $\lambda_0/2$  and  $\lambda_0/4$  transmission peaks; the folded Solc has a larger potential tuning range (wavelength units) than the fan Solc provided tuning is accomplished by variation of the  $\Delta n d$  product. Figure 21 contrasts the transmission spectrums for otherwise identical folded and fan Solc filters.

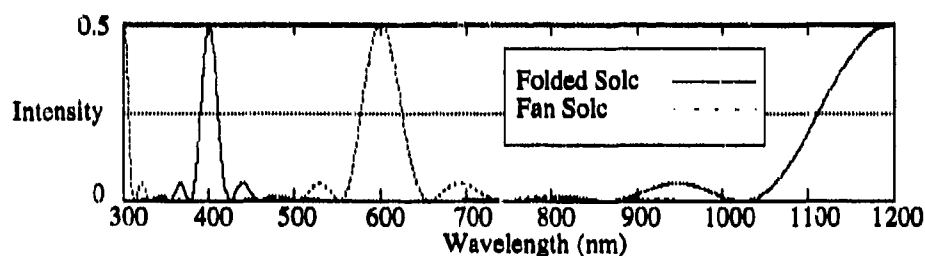


Figure 21. Transmission Spectrum for 10-plate Fan and Folded Solc Filters with Randomly Polarized Input ( $\Delta n d = 600$  nm)

Bandwidth calculation for the Solc filter requires some assumptions and approximations; first, we assume the wavelength is close to a wavelength where the plates are half-wave plates for the folded geometry or full-wave plates for the fan geometry. The assumption for the folded Solc filter is that  $(\lambda - \lambda_k) \ll \lambda_k$  where  $\lambda_k$  is the wavelength at which the retardance of each plate is  $(2k + 1)\pi$  and  $k = 0, 1, 2, 3$ , etc. For the fan geometry the retardance of each plate is  $(2k)\pi$  where  $k = 1, 2, 3$ , etc. When  $N \gg 1$  the FWHM bandwidth is given in [16] as:

$$BW_{\text{folded}} = \Delta\lambda_{1/2} \approx 1.60 \left( \frac{\lambda_k}{(2k+1)N} \right) \quad BW_{\text{fan}} = \Delta\lambda_{1/2} \approx 1.60 \left( \frac{\lambda_k}{(2k)N} \right) \quad (22)$$

From Equation 22 we can estimate the number of plates required to meet a given wavelength. From Equation 15 we can calculate the azimuth angle of the plates. Equation 18 determines the filter transmission peak wavelengths.

### The An-tuned Solc Filter

*Tuning Mechanism.* As with the standard Lyot filter, the transmission peaks of the Solc filter can be tuned by varying the product of  $\Delta n d$ ; usually the thickness "d" is fixed while  $\Delta n$  is changed. This analysis assumes that  $\Delta n$  is changed electrically via the electro-optic effect.

*Tuning Characteristics.* This discussion will concentrate on the folded Solc configuration and looks at filter characteristics such as tuning range, bandwidth, transmission, and rejection. Computer simulations and the equations above provide insight into the relationships between the filter characteristics.

As stated earlier, the maximum spectral distance between transmission peaks is between  $\lambda_0$  and  $\lambda_0/3$  where  $\lambda_0 = 2\Delta n d$ . If the shortest wavelength in the spectral range of interest is denoted  $\lambda_1$ , then we can increase  $\Delta n$  until  $\lambda = 3\lambda_1$  before a second

passband back at  $\lambda_1$  invades the spectral range. Thus, the maximum tuning range to maintain a single passband is slightly less than the spectral distance between  $\lambda_1$  and  $3\lambda_1$ . The bandwidth triples in this tuning scenario, as the filter is tuned from  $\lambda_1$  to  $3\lambda_1$ ; like the Lyot version, the bandwidth shows a linear variation with passband center wavelength. The next section illustrates the tuning characteristics of the  $\Delta n$ -tuned Solc filter with examples of HI system applications.

*Operation in the HI Spectral Region.* In this section the  $\Delta n$ -tuned Solc filter characteristics are analyzed for use in the HI spectral region. As mentioned earlier, the HI spectral range is 400 nm to 14.2  $\mu\text{m}$ . The shortest wavelength in the desired tuning range is 400 nm; the observations above and the equations for the folded Solc filter say that the upper wavelength is slightly less than three times the shortest wavelength (1.2  $\mu\text{m}$ ). The  $\Delta n$ -tuned Solc has almost the same tuning characteristics as the  $\Delta n$ -tuned Lyot. The exceptions are that the Solc has a 3:2 advantage in tuning range and higher side lobes, about 12 percent of peak main lobe transmission compared with about 5 percent for the Lyot. The folded Solc filter needs 64 half-wave plates to achieve close to a 10 nm bandwidth at the 400 nm pass band; the bandwidth grows to 30 nm when tuned to 1.2  $\mu\text{m}$  (Figure 22). If we use the same definition of a channel as that used in the Lyot discussion, the filter in Figure 22 will support 40 channels. A hypothetical set of filters is presented in Table 4.

#### The Wave-Plate-Tuned Solc Filter

*Tuning Mechanism.* This tuning method uses two achromatic quarter-wave plates and a rotatable achromatic half-wave plate per birefringent plate. The folded geometry is used in this discussion, but the wave-plate-tuning concept could also be applied to the fan geometry. The idea here is essentially the same as for the wave-plate-tuned Lyot, except the Solc needs the extra quarter-wave plate after the half-wave plate to maintain the

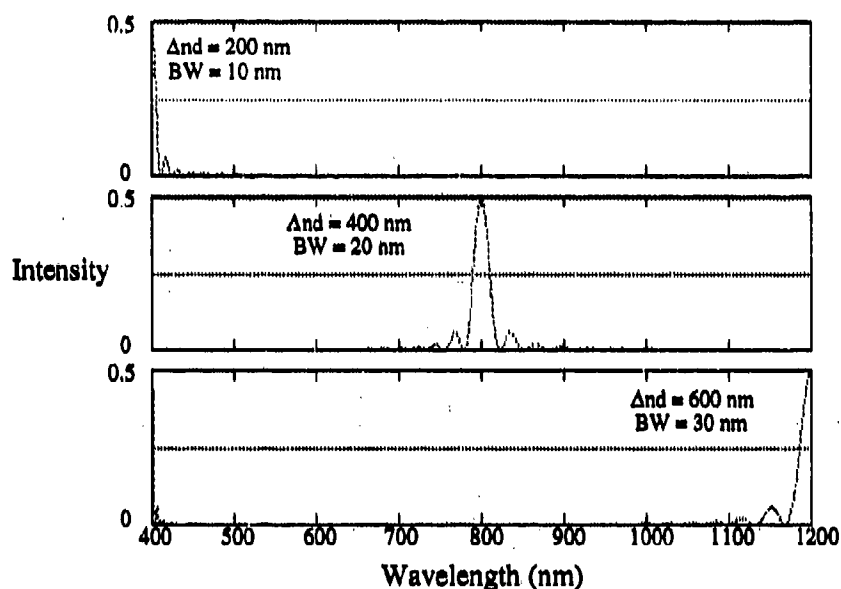


Figure 22. Tuning Characteristics for a 64-plate  $\Delta n$ -tuned Solc Filter in the Visible to Near Infrared Region

Table 4. A Set of  $\Delta n$ -tuned Solc Filters for the HI Spectrum

Tuning Range	Number of Stages	$\Delta n_1$ Range	Bandwidth Range (nm)	Maximum Channels
400 nm - 1.2 $\mu\text{m}$	64	200 nm - 600 nm	10 - 30	46
1.2 $\mu\text{m}$ - 3.0 $\mu\text{m}$	96	600 nm - 1.5 $\mu\text{m}$	20 - 50	50
3.0 $\mu\text{m}$ - 5.0 $\mu\text{m}$	96	1.5 $\mu\text{m}$ - 5 $\mu\text{m}$	50 - 83.3	30
7.0 $\mu\text{m}$ - 14.2 $\mu\text{m}$	64	3.5 $\mu\text{m}$ - 7.1 $\mu\text{m}$	175 - 355	27

proper phase relationship between the two orthogonal polarizations [17]. The tuning elements required for each element are shown in Figure 23; notice the number of plates required quadruples over the  $\Delta n$ -tuned Solc. As with the wave-plate-tuned Lyot, the quarter-wave plates are intended to be electrically rotated. Tuning the Solc filter with wave plates is a bit more complicated than tuning the Lyot version. The filter will act like a standard Solc when the azimuth angle of the half-wave plates are  $\rho + \pi/4$  for those birefringent plates with a positive angle (Figure 23a) and  $-\rho + \pi/4$  for those birefringent

plates with a negative angle (Figure 23b). The rotation angle of the half-wave-plates is the sum of the tuning angle " $\rho_t$ " and the angles just mentioned in the previous sentence;

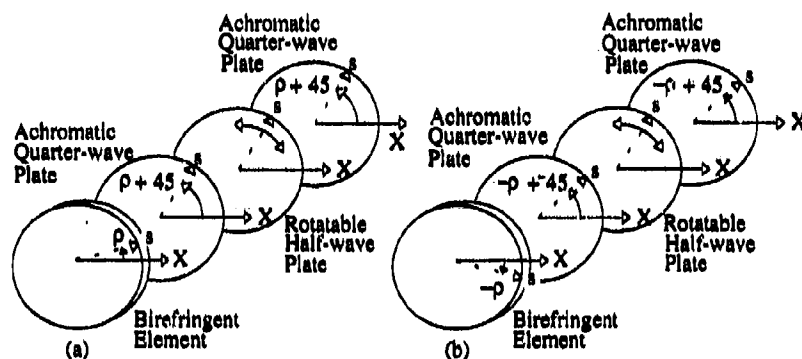


Figure 23. Birefringent Plates for the Folded Solc Filter with Associated Tuning Sections for (a) The Positive Azimuth Angle Plates (b) The Negative Angle Plates

theoretically, the filter will tune from a wavelength of  $2\Delta n d$  ( $\rho_t = 0$ ) to infinite wavelength ( $\rho_t = \pi/4$ ).

**Tuning Characteristics.** Computer simulations, expressions for the standard folded Solc filter, and knowledge gained in the study of the wave-plate-tuned Lyot filter provide insight into the wave-plate-tuned Solc filter. The bandwidth increases quadratically with pass band wavelength like the similarly tuned Lyot filter; Equation 22 does not apply for the bandwidth of the wave-plate-tuned Solc filter for any non zero  $\rho_t$ . The number of plates required for a specific bandwidth at the shortest filter wavelength is however calculated via Equation 22.

**Operation in the HI Spectral Region.** This filter requires 64 birefringent plates to achieve a 10 nm bandwidth at a 400 nm pass band; in addition 128 achromatic quarter-wave plates and 64 achromatic rotatable half-wave plates are needed to tune the filter. The spectral characteristics for the above mentioned filter were computer calculated and are presented in Figure 24. Even though this filter has sufficient tuning range to cover the

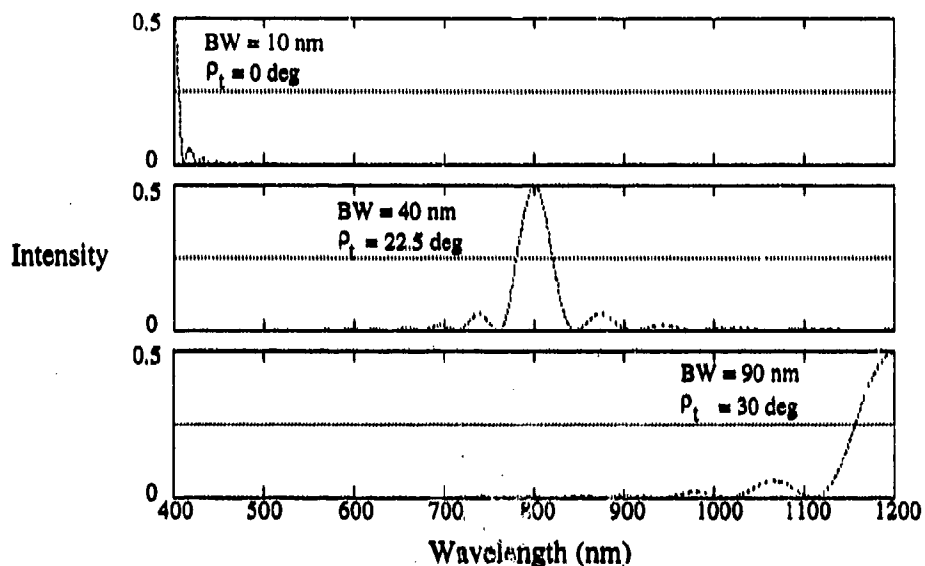


Figure 24. Tuning Characteristics for a 64-plate Wave-plate-tuned Solc Filter in the Visible to Near Infrared Region

entire HI spectral region, the quadratic bandwidth growth precludes tuning over such a large range. If we started with a 10 nm bandwidth while tuned to 400 nm, the bandwidth would be 12.6  $\mu\text{m}$  when tuned to 14.2  $\mu\text{m}$ ! For this reason, several filters would be needed to stay within the same order of magnitude of the HI bandwidth requirements defined in Chapter 1. A Hypothetical filter set is presented in Table 5.

Table 5. A Set of Wave-plate-tuned Solc Filters Required to Tune Over the HI Spectrum

Tuning Range	Number of Stages	$\Delta$ nd Product	Bandwidth Range (nm)	Maximum Channels
400 nm - 1.2 $\mu\text{m}$	96	200 nm	6.7 - 60	40
1.2 $\mu\text{m}$ - 3.0 $\mu\text{m}$	96	600 nm	20 - 125	36
3.0 $\mu\text{m}$ - 5.0 $\mu\text{m}$	96	1.5 $\mu\text{m}$	50 - 139	24
7.0 $\mu\text{m}$ - 14.2 $\mu\text{m}$	96	3.5 $\mu\text{m}$	117 - 480	30



### The Electro-optic Tunable Filter (EOTF)

*Tuning Mechanism.* The idea for the EOTF comes from a series of journal articles written by Pinnow, Lotspeich, and others [22], [23], [24], [25]. In these papers the filter discussed was constructed of a solid piece of birefringent material with several finger electrodes bonded to it (Figure 25). Various DC voltages were applied to the finger

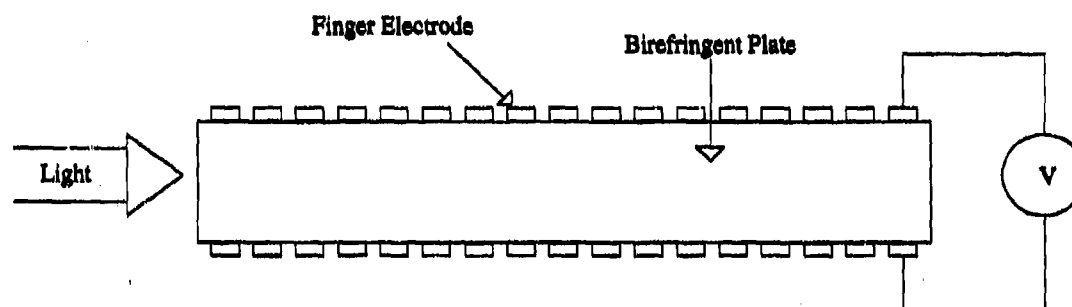


Figure 25. A Transverse-field Electro-optic Tunable Filter Proposed in [22]

electrodes; the voltages effectively changed the azimuth angle within each small section of the crystal via the electro-optic effect. This filter is tuned by changing the dc voltages applied across each pair of electrodes individually, with the individual voltages in a sinusoidal pattern. Much of the theory for this filter is borrowed from coupled wave theory used to explain the acousto-optic filter; however, Solc filter theory also provides insight. To see this, assume that  $\rho_{\max}$  in Figure 26 is equal to the Solc filter azimuth angle defined in Equation 15 with  $N$  equal to the number of electrode pairs. If we apply the angle pattern shown in Figure 26 to the filter of Figure 25 the filter acts like a Solc filter with the number of plates equal to the number of electrode pairs. In fact, this thesis uses separate birefringent plates instead of a solid piece of material to model this filter.

The Solc filter analogy only goes so far; to discuss tuning, some results from acousto-optic filters must be borrowed. This thesis makes no attempt to explain coupled

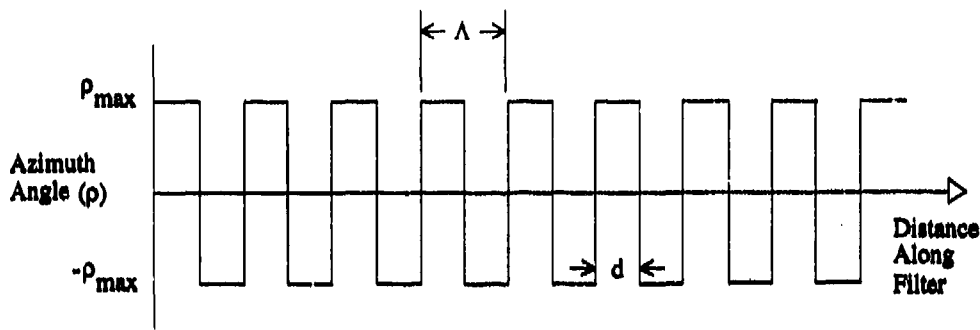


Figure 26. Voltage Waveform for Folded Solc Filter Operation, also Waveform for Shortest Pass Band Wavelength [22]

wave theory or acousto-optic filters; only results from these topics are used. For an explanation of the acousto-optic filter the reader is referred to [3] and [26]. For an explanation of solution of the coupled wave equations refer to [27], [28], and [29]. The EOTF and the acousto-optic filter share the same tuning relationship:

$$\lambda_0 = (n_i - n_o)\Lambda \quad (23)$$

where  $\lambda_0$  is the center pass band wavelength,  $n_i$  is the slow index of refraction,  $n_o$  is the fast index of refraction, and  $\Lambda$  is the spatial period of the field distribution within the filter. For the acousto-optic filter, the sinusoidal field distribution is set up by an acoustic wave; for the EOTF, the sinusoidal field disturbance is achieved by several discrete dc fields whose amplitudes follow a sampled sinusoidal pattern along the length of the filter (Figure 27). The maximum angle of the sinusoidal distribution " $\rho_{\max}$ " is not the same as for the Solc filter, except in the above mentioned case where  $\Lambda = 2d$  (when the EOTF acts like a folded Solc filter). Expressions for the transmission spectrum of the EOTF are

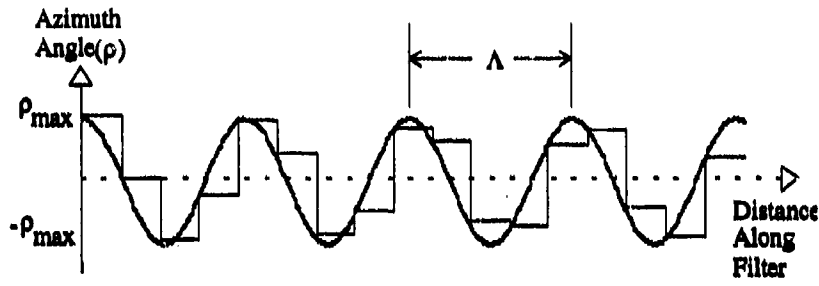


Figure 27. Sampled Cosine Wave Azimuth Angle Distribution for a Solc Filter

given in [23] and [24]. the expression for the transmission of the EOTF is:

$$T(\lambda, E_k) = \frac{\Gamma^2 \sin^2 \left[ \sqrt{\Gamma^2 + \delta^2} L \right]}{\Gamma^2 + \delta^2} \quad (24)$$

where  $L$  is the total birefringent material length,  $\Lambda$  is the coupling coefficient,  $\delta$  is the phase mismatch parameter, and  $E_k$  is the applied field strength. The expression from [23] for  $\Gamma$  is:

$$\Gamma = \pi(n_s n_r)^{3/2} r_{ijk} E_k 2\lambda \quad (25)$$

where  $E_k$  is the field strength applied to the crystal and

$$\delta = \pi(n_s - n_r) \left( \frac{1}{\lambda} - \frac{1}{\lambda_0} \right) \quad (26)$$

$r_{ijk}$  is the material electro-optic coefficient and  $\lambda_0$  is the pass band wavelength defined by Equation 23. The angle of eigen direction rotation " $\rho$ " as a result of an applied electric field is given in [23] as:

$$\tan 2\rho = \frac{2r_{ijk} E_k}{n_r^{-2} - n_s^{-2}} \quad (27)$$

To solve for  $\rho_{\max}$ , we first set  $\lambda = \lambda_0$  to ensure that transmission is at a peak; with  $\lambda = \lambda_0$ , and  $\delta = 0$ . Substituting this into Equation 24 we find that transmission is unity when  $\Lambda L = \pi/2$ . Using this fact, Equation 25, and Equation 23, yields an expression for the applied field required to have unity peak transmission.

$$E_k = \frac{\Lambda(n_s - n_f)}{L(n_s n_f)^{1/2} r_{ijk}} \quad \text{for} \quad \left( \lambda = \lambda_0, \quad \Gamma L = \frac{\pi}{2} \right) \quad (28)$$

Finally, substituting Equation 28 into Equation 27 produces an expression for  $\rho_{\max}$ .

$$\tan(2\rho_{\max}) = \frac{2\Lambda(n_s - n_f)}{(n_f^{-2} - n_s^{-2})(n_s n_f)^{1/2} L} \quad (29)$$

**Tuning Characteristics.** This section focuses on what happens to filter characteristics such as bandwidth as the filter is tuned. Also of prime importance is tuning range. This discussion assumes an EOTF made up of discrete plates with azimuth angles arranged in a sampled sinusoidal distribution. As eluded to above, the filter should tune smoothly from a fundamental shortest wavelength  $\lambda_f = 2\Delta n$  (when  $\Lambda = \lambda_f/\Delta n$ ) to longer wavelengths by increasing  $\Lambda$ . This is close to truth for wavelengths not close to  $\lambda_f$ . The actual spectral behavior of the filter as it is tuned is discussed using Fourier analysis in [25]. When the filter is tuned to  $\lambda_f$  with  $\rho_{\max}$  given by Equation 15, transmission is unity. If  $\Lambda$  is increased slightly, the passband at  $\lambda_f$  splits into two lower amplitude peaks, one on either side of  $\lambda_f$ . As  $\Lambda$  is further increased, the two peaks continue to move in opposite spectral directions. Figure 28 shows a computer simulation of pass band splitting where  $\lambda_0$  is the pass band center wavelength and  $\rho_{\max}$  is given by Equation 15. Another feature of this filter is its quadratic bandwidth growth with pass band center wavelength, similar to the wave-plate-tuned Lyot and Solc filters.

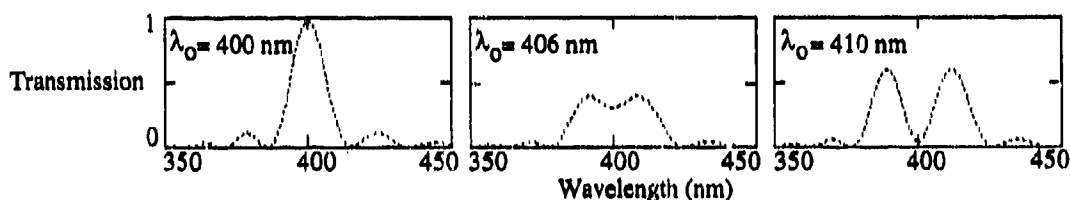


Figure 28. Computer Simulation of Pass Band Splitting Close to  $\lambda_f$  ( $\lambda_f = 400$  nm,  $N = 48$ )

*Operation in the HI Spectral Region.* Aside from its curious behavior near  $\lambda_f$ , the ETOF has characteristics similar to the wave-plate-tuned Solc filter. To illustrate some of the subtle differences, consider an EOTF with  $\lambda_f = 380$  nm, 48 plates, and a desired tuning range whose shortest wavelength is 400 nm. The maximum azimuth angle " $\rho_{\max}$ " is given by Equation 29. Figure 29 is a computer simulation of such a filter. One

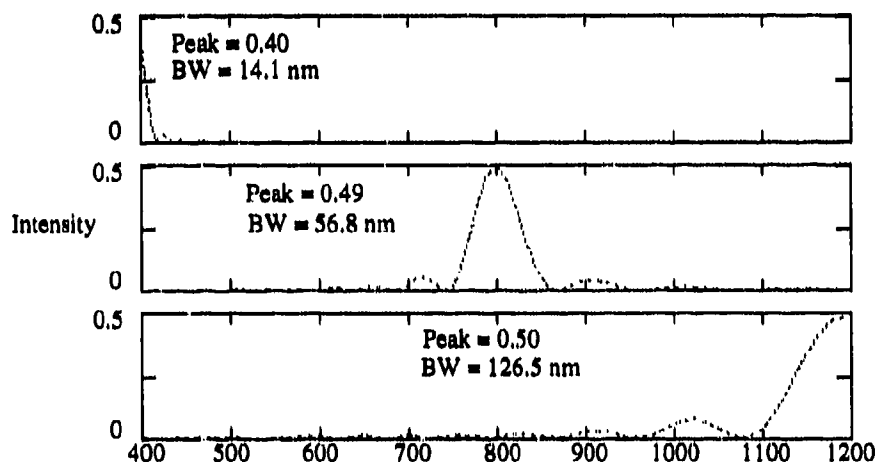


Figure 29. Tuning Characteristics for a 48-plate EOTF Filter with Randomly Polarized Input in the Visible to Near Infrared Region ( $\Delta n_d = 190$  nm,  $\rho_{\max}$  given by Equation 29)

difference between the wave-plate-tuned Solc and the EOTF is that the transmission drops off close to  $\lambda_f$  for the EOTF. The other difference is that  $\Delta n_d$  for each plate must be

slightly less than  $\Delta n d$  for the wave-plate-tuned Solc filter in order to have smooth tuning from the same short wavelength limits. Figure 31 shows how peak transmission falls off close to the short wavelength limit of the filter.

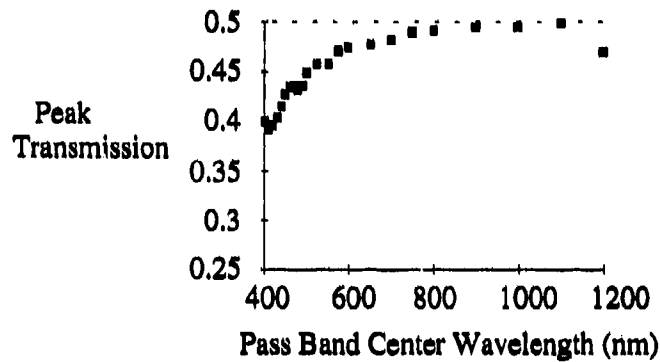


Figure 30. Computer Simulation for Pass Band Center Wavelength versus Transmission at Pass Band Peak ( $\Delta n d = 190$  nm,  $N = 48$ ,  $\rho_{\max}$  given by Equation 29)

A set of filters almost identical in filtering characteristics to the wave-plate-tuned Solc filters in Table 5 are presented in Table 6 for the EOTF. The EOTF does have one

Table 6. A Set of EOTFs Required to Tune Over the HI Spectrum

Tuning Range	Number of Plates	$\Delta n d$ Product	Bandwidth Range (nm)	Maximum Channels
400 nm - 1.2 $\mu\text{m}$	96	190 nm	7 - 63	38
1.2 $\mu\text{m}$ - 3.0 $\mu\text{m}$	96	580 nm	21 - 129	34
3.0 $\mu\text{m}$ - 5.0 $\mu\text{m}$	96	1.44 $\mu\text{m}$	52 - 144	23
7.0 $\mu\text{m}$ - 14.2 $\mu\text{m}$	96	3.4 $\mu\text{m}$	120 - 493	29

notable advantage over the wave-plate-tuned Solc in the total number of elements required; the EOTF requires no extra elements to achieve tuning.

### Pass Band Shaping with Solc-type Filters

*Solc Sections Joined with Polarizers.* The multiple Solc filter consists of Solc sections separated by polarizers (Figure 31), similar to a Lyot filter whose birefringent

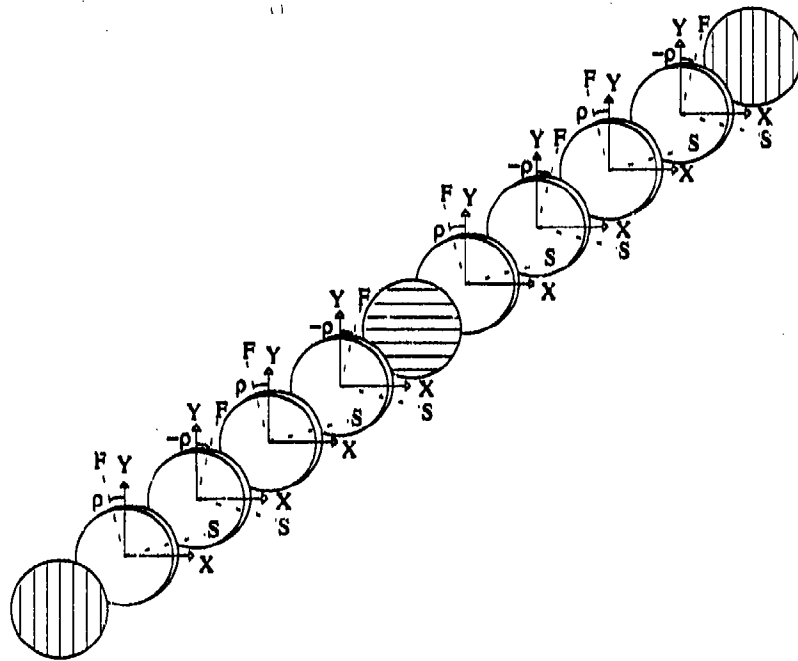


Figure 31. Two 4-stage Solc filters Cascaded with a Polarizer

elements are replaced by several identical wave plates in a Solc configuration [17]. The question is: Do combinations of Solc filters offer any advantages over the standard Solc or Lyot? Figure 32 shows a computer simulation for a filter made up of two 6 plate Solc sections separated by a polarizer compared with a single Solc filter of 12 identical plates. The first folded Solc section of the double Solc filter has plates with a  $\Delta n d$  product of 400 nm; the other Solc section has six plates whose thickness is 9 $\Delta n d$  or nine times as thick as the plates in the first section. When the two Solc sections are cascaded via a polarizer, their two output spectra multiply as in a Lyot filter. The result is that the relatively wide free spectral range is set by the thin-plate section while the narrow

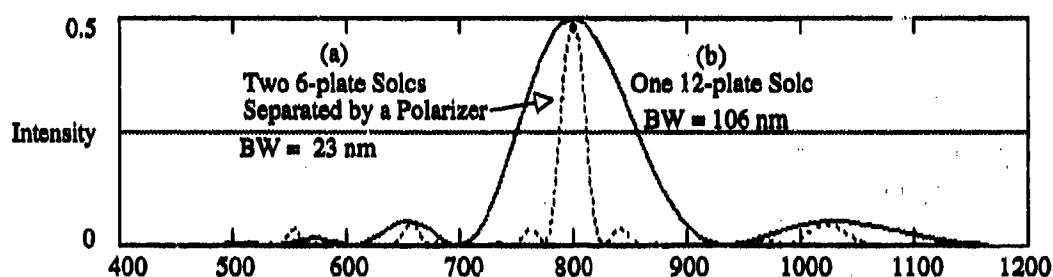


Figure 32. Computer Simulation Contrasting Two 12-plate Filters (a) Two 6-plate Solc Sections Joined by a Polarizer (plate thickness is  $d$  for one section and  $9d$  for the other) (b) One 12-plate Solc filter (thickness =  $d$  for all elements)

bandwidth is dictated by the thick-plate section. Of course there is a limit to the thickness ratio between the first stage plates and the second stage plates. The 1:9 ratio here while exhibiting a high free spectral range to bandwidth ratio, shows many significant side lobes. The side lobes could be reduced by adding a third stage of intermediate thickness, or by making the thicknesses of the two stages closer. However, adding a third stage increases the number of plates and reducing the thickness ratio hurts the free spectral range to bandwidth ratio. The number of stages, plates, and polarizers can always be traded for large free spectral range, narrow bandwidth, better side lobe characteristics. As with the standard Lyot or Solc filter,  $\Delta n$ -tuning, and wave-plate-tuning are possible.

*Optical Network Synthesis.* Harris, Ammon, and Chang made an important contribution to optical filtering by devising a procedure to synthesize arbitrary pass band shapes with two polarizers and identical birefringent elements [30]. The procedure allows the filter designer to specify an arbitrary output response and to design a filter to produce that output response. The desired output response is put in the form of a truncated Fourier series; the inverse Fourier transform of the output response is the impulse response of the filter. The procedure translates the individual terms of the impulse response into the azimuth angles of the output polarizer and each birefringent element.



This is an admittedly simplified explanation with few details; for full explanation refer to [30].

Filters designed with this technique produce excellent pass band characteristics and side lobe suppression. However, the Fourier series (and inverse Fourier series) of an ideal periodic rectangular passband has an infinite number of terms. An infinite number of plates are required to synthesize such an output spectrum. The more the series is truncated, the more distorted the output response becomes through higher side lobes, and gradual roll-off. In short, improvements in pass band characteristics cost more plates.

This filter can be  $\Delta n$ -tuned or wave-plate-tuned although it doesn't offer anything in the way of bandwidth control as the filter is tuned to longer wavelengths. The bandwidth versus center wavelength relationship is essentially the same as the similarly tuned Solc filter.

## IV. Conclusions and Recommendations

### Introduction

This thesis considered two broad classes of electrically tunable birefringent optical filters for application to HI systems, Lyot based filters and Solc based filters. Chapter 1 defined the thesis problem, laid the HI system groundwork, defined an ideal TOF for HI application, and briefly discussed the limitations and methodology of this thesis. Chapter 2 discussed the findings for the Lyot based filters and Chapter 3 discussed Solc based filters. Two possible tuning mechanisms provided band pass spectral agility for the Lyot class of filters,  $\Delta n$ -tuning and wave-plate-tuning; Chapter 2 addressed both tuning methods. The two Lyot tuning methods also apply to the Solc filters and are analyzed in Chapter 3. The EOTF, in Chapter 3, introduced a third tuning method; this tuning method relies on the spatial period of the azimuth angle envelope for tuning. Analytical expressions and computer simulations evaluated tuning, bandwidth, and transmission characteristics for filters of both classes in their respective chapters.

### Conclusions for Tunable Optical Filters

*The  $\Delta n$ -tuned Lyot Filter.* One of this filter's strong points for HI application include its simplicity; relatively few birefringent elements are needed to achieve HI type bandwidths and it requires no "extra" tuning elements. Bandwidth (in wavelength) grows linearly with pass band center wavelength which is better than the quadratic growth of some other filters, but not constant like the ideal filter defined. The major detractor of this filter concept is its relatively narrow tuning range; the  $\Delta n$ -tuned Lyot filter can only tune from  $\Delta n_1$  to  $2\Delta n_1$  and this assumes a doubling  $\Delta n$ . This tuning range is probably too small for HI applications.

*The Wave-plate-tuned Lyot Filter.* Theoretically, this filter can tune from  $\Delta n_1$  to any longer wavelength which makes the tuning range almost unlimited. Even though the

wave-plate-tuned Lyot filter can theoretically tune over the entire HI spectral range (400 nm - 14.2  $\mu\text{m}$ ), its bandwidth characteristics and the practical rotation limits of the tuning elements preclude a tuning range this wide. The bandwidth grows quadratically with center wavelength; a bandwidth of 10 nm at a 400 nm pass band becomes 90 nm at 1.2  $\mu\text{m}$ . Another negative feature of this filter is that it needs two tuning elements per birefringent filter element, triple the number of elements of the  $\Delta n$ -tuned Lyot filter.

*The  $\Delta n$ -tuned Solc Filter.* This filter acts much like the  $\Delta n$ -tuned Lyot filter with the exception of the tuning range. The theoretical tuning range goes from the shortest filter wavelength ( $2\Delta n d$ ) to three times the shortest filter wavelength a 3:2 advantage over the Lyot filter. Birefringent wave plates for this filter need to have a wide range of the  $\Delta n d$  product; the product must triple to take advantage of the full tuning range. The bandwidth grows linearly with pass band center wavelength which is the best any of the filters considered in this thesis can do. The  $\Delta n$ -tuned Solc filter uses only two polarizers, but many more birefringent plates than the Lyot filter. Total reflection losses would be high due to the high number of plates required. Additionally,  $\Delta n d$  must be small at the shorter wavelengths, as small as 200 nm. If the shortest wavelength  $\Delta n$  is 0.05, this would mean a plate thickness of 4  $\mu\text{m}$  and  $\Delta n$  must be capable of increasing to 0.15.

*The Wave-plate-tuned Solc Filter.* This filtering concept needs an extraordinary number of elements to approach HI spectral characteristics; the examples in Table 5 use 96 birefringent elements with three extra tuning elements needed for each stage for a total of 384 elements. In addition, its tuning characteristics are similar to the wave-plate-tuned Lyot filter; its bandwidth grows quadratically with pass band wavelength. Even if a solution is found for the quadratic bandwidth growth, the wave-plate-tuned Solc filter is a poor candidate for HI application.

*The EOTF.* This clever extension of acousto-optic filter theory is plagued by the same bandwidth problem that the wave-plate-tuned filters are, quadratic bandwidth

dependence on center wavelength. Its tuning characteristics are unique among the filters considered in this thesis, with pass band splitting near the fundamental filter wavelength " $\lambda_f$ ". Other than the behavior close to  $\lambda_f$ , the tuning characteristics are much like the wave-plate-tuned filters. Although the computer simulations for this filter were accomplished using separate birefringent plates, a single piece of material has been used to fabricate the EOTF [22]. Single crystal construction makes this filter attractive from a fabrication standpoint.

*Pass Band Shaping Filters.* Filters or filtering concepts discussed in this category were the Lyot filter with contrast element, the Lyot filter with non-standard plate thicknesses, the two stage Solc filter, and a Lyot and Solc technique for producing arbitrary pass band shapes.

The Lyot filter with contrast element was considered as a means to suppress side lobes. The computer simulation (Figure 16) showed about a five-fold reduction in the main side lobes for the specific wavelength range used. If one of the Lyot filters considered above found use as a spectral discriminator for some type of detector, side lobe suppression would be useful to increase the signal to noise ratio.

The Lyot filter with non-standard plate thickness shows that the standard Lyot thickness ratios are alterable. Using this idea, results of a computer simulation (17) show that it is possible to achieve a narrower bandwidth than the standard Lyot filter without using more plates; however, the sidelobes were higher than the standard Lyot filter. Non-standard plate thickness might also be used to suppress side lobes with other thickness combinations.

Arbitrary pass band shapes can be accomplished in theory. The partial polarizer method uses a Lyot arrangement while the optical network synthesis procedure relies on a Solc type arrangement. Pass band shaping offers the potential to eliminate undesirable transmission characteristics such as side lobes, but comes at the expense of more

elements. A filter designed with this technique would almost certainly be tunable using either  $\Delta n$ -tuning or wave-plate-tuning; however, tuning characteristics won't improve over the filters already discussed. Wave-plate tuning would exhibit quadratic bandwidth growth with center pass band wavelength and  $\Delta n$ -tuning would limit tuning range.

### Recommendations for Further Research

*General Considerations.* This thesis looked at potential electro-optically tuned birefringent filters. Another major class of birefringent filters, acousto-optic filters, was not considered and for completeness should be. Filter and tuning elements used in this thesis are loosely based on existing technology; however, material constraints were largely ignored and this thesis made no attempt to identify specific materials for any of the birefringent elements or polarizers. Even assuming ideal material characteristics, the filters considered in this thesis are poor candidates for HI applications as defined. However, filters investigated might prove useful for non-HI applications where bandwidth control is not important and where tuning ranges are narrower.

*Filter Research.* Collinear and non-collinear acousto-optic filters should be evaluated for HI application. Arbitrary band shape filters based on the lossy polarizer concept and the optical network synthesis technique should be further investigated with an eye toward HI application and possible new tuning techniques.

*Material Research.* If a less restrictive application for birefringent tunable optical filters arises, Research should be conducted to determine the actual capabilities of the filters investigated in this thesis with currently available birefringent and polarizer materials. Birefringent material properties such as the range of  $\Delta n$  and the amount of eigen direction rotation possible through the electro-optic effect should be researched. Also, "thin" wave-plates should be addressed to determine available thicknesses and techniques to achieve thin birefringent layers. Achromatic waveplates should be

characterized to determine the spectral range over which they are close enough to achromatic to be of use.

*Other Research.* Further research should include radiometric and detection analysis to determine signal-to-noise ratios required for HI applications and how a given optical filter would affect the actual signal-to-noise ratio. Since bandwidth considerations played such major role in the evaluation of the filters in this thesis, bandwidth requirements should be scrutinized from the earth sciences and remote sensing points of view to see if requirements could be relaxed without affecting data usefulness.

## References

- [1] Lyot, B. "Optical Apparatus with Wide Field Using Interference of Polarized Light," Comptes Rendus, 197: 1593 (1933).
- [2] Solc, I. Czechoslovakian Journal of Physics, 3: 366 (1953); 4: 607, 669 (1954); 5: 114 (1955).
- [3] Harris, S. E. and R.W. Wallace. "Acousto-optic Tunable Filter," Journal of the Optical Society of America, 59: 744-747, (June 1969).
- [4] Slater, Philip N. Remote Sensing Optics and Optical Systems. Reading MA: Addison-Wesley Publishing Company, 1980.
- [5] Colwell, Robert N. Manual of Remote Sensing (Second Edition). Falls Church VA: American Society of Photogrammetry, 1983.
- [6] Goddard Space Flight Center. EOS Reference Handbook. U.S. Government Printing Office, 1990.
- [7] Salomonson, Vincent V. and others. "MODIS: Advanced Facility Instrument for Studies of the Earth as a System," IEEE Transactions on Geoscience and Remote Sensing, 27: 145-152 (March 1989).
- [8] Irons, James R. and others. "Advanced Solid-State Array Spectroradiometer (ASAS) support of 1989 field experiments," Proceedings of SPIE - The International Society for Optical Engineering, 1298: 2-10 (April 1990).
- [9] Goetz, Alexander F. and Mark Herring. "The High Resolution Imaging Spectrometer (HIRIS)," IEEE Transactions on Geoscience and Remote Sensing, 27: 136-143 (March 1989).
- [10] Baudin, Gilles and Richard Bessudo. "Medium Resolution Imaging Spectrometer (MERIS)," Proceedings of SPIE - The International Society for Optical Engineering, 1490: 102-113 (April 1991).
- [11] Rees, W. G. Physical Principles of Remote Sensing. Cambridge: Cambridge University Press, 1990.
- [12] Iwasaki, Nobuo and others. "Mission Overview of ADEOS Program," Proceedings of SPIE - The International Society for Optical Engineering, 1490: 192-199 (April 1991).

- [13] Boyd, Robert W. Radiometry and the Detection of Optical Radiation. New York NY: John Wiley and Sons, 1983.
- [14] Jones, R. C. "New calculus for the Treatment of Optical Systems," Journal of the Optical Society of America, 31: 488, (1941).
- [15] Hecht, E. Optics (Second Edition). Reading, MA: Addison-Wesley Publishing Company, 1987.
- [16] Yariv, A. and P. Yeh. Optical Waves in Crystals. New York NY: John Wiley and Sons Inc., 1984.
- [17] Title, A. M. and W. J. Rosenberg. "Tunable Birefringent Filters," Optical Engineering, 20: 815-823 (November/December 1981).
- [18] Sharp, G. D. and others. "Continuously Tunable Smectic A\* Liquid-crystal Color Filter," Optics Letters, 15: 523-525, (May 1990).
- [19] Bair, C. H. "Birefringent Filter Design," United States Patent 5,062,694, (November 5, 1991).
- [20] Ammann, E. O. and I.C. Chang. "Optical Network Synthesis using Birefringent Crystals. II. Synthesis of Networks Containing One Crystal, Optical Compensator, and Polarizer per Stage\*," Journal of the Optical Society of America, 55: 835-841, (July 1965).
- [21] Title, A. M. "Improvement in Birefringent Filters. 4: The Alternate Partial Polarizer Filter," Applied Optics, 15: 2871-2879, (November 1976).
- [22] Pinnow, D. A. and others. "An Electro-optic Tunable Filter," Applied Physics Letters, 34: 391-393, (March 1979).
- [23] Lotspeich, J. F. and others. "Electro-optic Tunable Filter," Optical Engineering, 20: 830-836, (November/December 1981).
- [24] Lotspeich, J. F. and others. "Electrooptic Tunable Filters for Infrared Wavelengths," IEEE Journal of Wuantum Electronics, OE-18: 1253-1258, (August 1982).
- [25] Lotspeich, J. F. and others. "Harmonic Response of a Tunable Solc Filter," Applied Optics, 22: 2743-2746, (September 1983).



- [26] DePriest, C. D. "Theoretical Investigations of a Tunable Collinear Acousto-optic Filter," Master's thesis, Air Force Institute of Technology, Wright-Patterson Air Force Base OH, (March 1985).
- [27] Yeh, P. "Transmission Spectrum of a Solc Filter," Optical Communications, 29: 1-6, (April 1979).
- [28] Yariv, A. "Coupled-node Theory for Guided-wave Optics," IEEE Journal of Quantum Electronics, OE-9: 919-933, (September 1973).
- [29] Marcuse, D. "Electrooptic Coupling Between TE and TM Modes in Anisotropic Slabs," IEEE Journal of Quantum Electronics, OE-11: 759-767, (September 1975).
- [30] Harris, S. E. and others. "Optical Network Synthesis Using Birefringent Crystals.\* I. Synthesis of Lossless Networks of Equal Length Crystals," Journal of the Optical Society of America, 54: 1267-1279, (October 1964).

### Vita

Captain Duane A. Sauve was born on 22 January 1961 in Burien, Washington. He graduated from Helena High School in Helena, Montana in 1979. He enlisted in the U. S. Air Force in 1983 and after a two year tour at McChord AFB in Washington was selected for the Airman's Education and Commissioning Program in 1985. He graduated from the University of Nebraska at Lincoln in May 1988 with a Bachelor of Science degree in Electrical Engineering then attended Officer Training school. Upon graduation in September of 1988, he was commissioned in the USAF and assigned to the 6510 Test Group and later to the 6518 Test Squadron at Edwards AFB, California where he was a Flight Test Engineer on the Combat Talon II special operations aircraft and AC-130U Gunship. He remained at Edwards until entering the School of Engineering, Air Force Institute of Technology, in May 1992.

**Permanent Address:**

**8410 Applegate Drive**

**Helena, Montana 59601**

REPORT DOCUMENTATION PAGE			Form Approved OMB No. 0704-0188	
Public reporting burden for this collection of information is estimated to average 1 hour per response, including the time for reviewing instructions, searching existing data sources, gathering and maintaining the data needed, and completing and reviewing the collection of information. Send comments regarding this burden estimate or any other aspect of this collection of information, including suggestions for reducing this burden, to Washington Headquarters Services, Directorate for Information Operations and Reports, 1215 Jefferson Davis Highway, Suite 1204 Arlington, VA 22202-4302, and the Office of Management and Budget, Paperwork Reduction Project (0704-0188), Washington, DC 20503.				
1. AGENCY USE ONLY (Leave blank)	2. REPORT DATE <b>December 1993</b>	3. REPORT TYPE AND DATES COVERED <b>Master's Thesis</b>		
4. TITLE AND SUBTITLE <b>A THEORETICAL INVESTIGATION OF ELECTRICALLY TUNABLE BIREFRINGENT OPTICAL FILTERS AS THE SPECTRAL DISCRIMINATOR IN HYPERSPECTRAL IMAGING SYSTEMS</b>		5. FUNDING NUMBERS		
6. AUTHOR(S) <b>Duane A. Sauve, Captain, USAF</b>				
7. PERFORMING ORGANIZATION NAME(S) AND ADDRESS(ES) <b>Air Force Institute of Technology, WPAFB OH 45433-6583</b>		8. PERFORMING ORGANIZATION REPORT NUMBER <b>AFTT/GEO/ENP/93D-02</b>		
9. SPONSORING/MONITORING AGENCY NAME(S) AND ADDRESS(ES) <b>Rome Laboratories OCPC Griffiss AFB, NY 13441</b>		10. SPONSORING/MONITORING AGENCY REPORT NUMBER		
11. SUPPLEMENTARY NOTES				
12a. DISTRIBUTION/AVAILABILITY STATEMENT  <b>Approved for public release; distribution unlimited</b>		12b. DISTRIBUTION CODE		
13. ABSTRACT (Maximum 200 words)  <b>This study investigated electrically tunable birefringent optical filters for use as the spectral discriminator in hyperspectral imaging systems. Spectral discrimination requirements for hyperspectral imaging systems were defined using specification from two state-of-the-art hyperspectral imaging systems. The spectral discrimination requirements led to the definition of the ideal tunable optical filter for spectral discrimination purposes. Analytical and computer analysis was performed for known birefringent filters which showed promise of electrical tunability, excluding acousto-optic filters. No perfect match was found to the ideal tunable optical filter for hyperspectral imaging defined in this thesis. Both Lyot and Solc based filters exhibited two drawbacks for hyperspectral imaging application: narrow tuning range with linear bandwidth dependence on center wavelength, or wide tuning range and quadratic bandwidth dependence on center wavelength. The <math>\Delta n</math>-tuned Solc filter provided the best compromise between tuning range and bandwidth control; however, it is not practical due to the excessive number of elements required. This thesis provides the needed background for further research in this area and identifies a number of areas for further worthwhile research. Acousto-optic filters offer another possible avenue for hyperspectral imaging and should be investigated. Birefringent materials should also be studied to determine material limits on the electro-optic effect and spectral transmission characteristics to determine practical capabilities of filters discussed in this thesis.</b>				
14. SUBJECT TERMS  <b>Birefringence, Filters, Multispectral, Imaging, Optical Filters</b>		15. NUMBER OF PAGES <b>66</b>		16. PRICE CODE
17. SECURITY CLASSIFICATION OF REPORT <b>Unclassified</b>	18. SECURITY CLASSIFICATION OF THIS PAGE <b>Unclassified</b>	19. SECURITY CLASSIFICATION OF ABSTRACT <b>Unclassified</b>	20. LIMITATION OF ABSTRACT <b>UL</b>	

## GENERAL INSTRUCTIONS FOR COMPLETING SF 298

The Report Documentation Page (RDP) is used in announcing and cataloging reports. It is important that this information be consistent with the rest of the report, particularly the cover and title page. Instructions for filling in each block of the form follow. It is important to *stay within the lines* to meet optical scanning requirements.

**Block 1. Agency Use Only (Leave blank).**

**Block 2. Report Date.** Full publication date including day, month, and year, if available (e.g. 1 Jan 88). Must cite at least the year.

**Block 3. Type of Report and Dates Covered.** State whether report is interim, final, etc. If applicable, enter inclusive report dates (e.g. 10 Jun 87 - 30 Jun 88).

**Block 4. Title and Subtitle.** A title is taken from the part of the report that provides the most meaningful and complete information. When a report is prepared in more than one volume, repeat the primary title, add volume number, and include subtitle for the specific volume. On classified documents enter the title classification in parentheses.

**Block 5. Funding Numbers.** To include contract and grant numbers; may include program element number(s), project number(s), task number(s), and work unit number(s). Use the following labels:

C - Contract	PR - Project
G - Grant	TA - Task
PE - Program Element	WU - Work Unit Accession No.

**Block 6. Author(s).** Name(s) of person(s) responsible for writing the report, performing the research, or credited with the content of the report. If editor or compiler, this should follow the name(s).

**Block 7. Performing Organization Name(s) and Address(es).** Self-explanatory.

**Block 8. Performing Organization Report Number.** Enter the unique alphanumeric report number(s) assigned by the organization performing the report.

**Block 9. Sponsoring/Monitoring Agency Name(s) and Address(es).** Self-explanatory.

**Block 10. Sponsoring/Monitoring Agency Report Number.** (If known)

**Block 11. Supplementary Notes.** Enter information not included elsewhere such as: Prepared in cooperation with...; Trans. of...; To be published in... When a report is revised, include a statement whether the new report supersedes or supplements the older report.

**Block 12a. Distribution/Availability Statement.** Denotes public availability or limitations. Cite any availability to the public. Enter additional limitations or special markings in all capitals (e.g. NOFORN, REL, ITAR).

DOD - See DoDD 5230.24, "Distribution Statements on Technical Documents."

DOE - See authorities.

NASA - See Handbook NHB 2200.2.

NTIS - Leave blank.

**Block 12b. Distribution Code.**

DOD - Leave blank.

DOE - Enter DOE distribution categories from the Standard Distribution for Unclassified Scientific and Technical Reports

NASA - Leave blank.

NTIS - Leave blank.

**Block 13. Abstract.** Include a brief (*Maximum 200 words*) factual summary of the most significant information contained in the report.

**Block 14. Subject Terms.** Keywords or phrases identifying major subjects in the report.

**Block 15. Number of Pages.** Enter the total number of pages.

**Block 16. Price Code.** Enter appropriate price code (*NTIS only*).

**Blocks 17. - 19. Security Classifications.** Self-explanatory. Enter U.S. Security Classification in accordance with U.S. Security Regulations (i.e., UNCLASSIFIED). If form contains classified information, stamp classification on the top and bottom of the page.

**Block 20. Limitation of Abstract.** This block must be completed to assign a limitation to the abstract. Enter either UL (unlimited) or SAR (same as report). An entry in this block is necessary if the abstract is to be limited. If blank, the abstract is assumed to be unlimited.